AN ABSTRACT OF THE THESIS OF

Tobias Siegfried Bathon for the degree of Master of Science in Electrical and Computer Engineering presented on July 8, 1999. Title: Passively Controlled Variable-Speed Generator System.

Redacted for Privacy

Abstract approved: _____

Alan K. Wallace

This thesis presents both an analysis and simulations of a passively controlled variable-speed generator system, which can be applied for renewable energy sources such as wind turbines. Parallel connected passive/external resistors and inductors are connected to the slip rings of a wound rotor induction machine to provide an acceptable speed operation range, while maintaining high efficiency of the generator system. Two generators, of 80 kW and 186 kW ratings, have been tested and compared to their simulations and good correlation has been obtained.

It is shown by both modelling and by laboratory tests that the steady-state power characteristic is well suited to the application and the efficiency compares well with similar rated machines in which either a fixed speed is required or power electronic converters provide the adjustable speed control. Thus, the tested systems are comparable in energy capture while being lower in costs and being both more robust and more reliable. In consequence, it is a more practical solution than power electronics for remote locations.

The dynamic results indicate that the generator is dynamically stable following three types of transient conditions: connections to the grid at non-synchronous speed; sudden decreases and increases in applied torque to simulate wind gusts; cyclic torque changes to demonstrate tower shadow effects. Unreasonable transients and undamped conditions have been neither predicted nor observed.

Finally, it is proposed that the external elements could be developed to be linked to the rotor circuit without slip rings enabling a complete passive and brushless system.

Passively Controlled Variable-Speed Generator System

by

Tobias Siegfried Bathon

A THESIS

submitted to

Oregon State University

in partial fulfillment of
the requirements for the
degree of

Master of Science

Presented July 8, 1999
Commencement June 2000

Master of Science thesis of Tobias Siegfried Bathon presented on July 8, 1999.

APPROVED :

Redacted for Privacy

Major Professor, representing Electrical and Computer Engineering

Redacted for Privacy

Head of the Department of Electrical and Computer Engineering

Redacted for Privacy

Dean of the Graduate School

I understand that my thesis will become part of the permanent collection of Oregon State University libraries. My signature below authorises release of my thesis to any reader upon request.

Redacted for Privacy

Tobias Siegfried Bathon, Author

ACKNOWLEDGEMENTS

I wish to thank my major professor, Dr. Alan Wallace, who supported and guided me in his friendly "British" nature throughout my graduate work and whose knowledge and advice were so important for this accomplishment. A special thanks goes to his trust in me from the day we have met in Portland.

I would also like to thank Dr. Annette von Jouanne, Dr. Molly Shor, and Dr. Dean Jensen for their friendly cooperation, review of my thesis, and for participating on my committee.

I also wish to thank Dr. Ion Boldea for his help and valuable ideas regarding my dynamic simulations and for the so interesting conversations and wise advice for life, which will help me, I'm sure, over the "Long Run".

Well, a special thanks goes to the folks at the motor lab, Richard Jeffreys, Fahad Al-ghubari, Manfred Dittrich, Jerry Duncan, Marcel Merk, Prabha Krishna Atluri, and Evelyn Matheson, who helped me throughout my research and studies and who partly shared with me these uncomfortable feelings when "Loud Bangs and Smoke" occurred.

Table of Contents

Page

Table of Contents (Continued)

Page

LIST OF FIGURES

LIST OF FIGURES (Continued)

LIST OF TABLES

DEDICATION

I dedicate this work to my family,
who have taught me life and "Schoofskopp", and of whom I'm so proud:

Guido, Rosi,
Christian, Leander, and Albrecht.

PASSIVELY CONTROLLED VARIABLE-SPEED GENERATION SYSTEM

1. INTRODUCTION

In order to supplement base load generation from fossil fuel, nuclear powered thermal plants, and conventional hydro stations, renewable energy sources such as low-volume hydro, wind turbines, and ocean-wave systems are being developed [1]. These are diffuse energy sources, of variable magnitude and speed for which efficient energy capture and minimum possible equipment capital cost are important for viability. To attain these conflicting goals, several systems are being investigated throughout the world. The possible alternative energy conversion processes, particularly for wind turbines, is shown schematically in Fig. 1.1 [1]. Apart from the wind turbine itself, the gearboxes and power electronic converters account for the major components of capital cost. For maximum system efficiency, the potential of direct drive and novel configurations of synchronous machines using permanent magnets and complex power electronic controllers is obvious [2-4]. However, the structural, electromagnetic and electronic development problems and resultant high capital cost of these systems may prove prohibitive. Although induction machines are generally a few percentage points less efficient than synchronous machines of comparable rating, they are only practical with small pole numbers (2 through 8) because of worsening power factors and, consequently, induction generators usually require gearboxes at the low speeds developed by wind turbines. If the concept of doubly-fed induction generator operation is employed, the rating of the required power electronic converters can be substantially reduced from that of the total system rating [5-7] thus off-setting gearbox costs. However, doubly-fed wound-rotor induction machines introduce the requirement for slip-rings and brushes which, under variable-speed and changing current density operation, have reliability/maintenance implications. Another alternative [8, 9] proposes passive control of doubly-fed induction machines with the additional advantages of robustness, lower capital cost, very high power quality, and ease of maintenance. This thesis investigates

the use of passive wound-rotor induction generator control, and reports on simulations and practical tests of an 80 kW and a 186 kW unit.

The analyzed generator system consists basically of a slip-ring wound rotor induction machine and passive/external resistors and inductors. As is well described in this thesis, the speed operation of the generator can be extended by connecting a parallel configured resistor and inductor over slip-rings to the rotor circuit. Future studies may be undertaken to mount those external/passive elements directly on the shaft of the generator to overcome those slip-ring and brush systems, which demand maintenance and increase the mechanical loss.

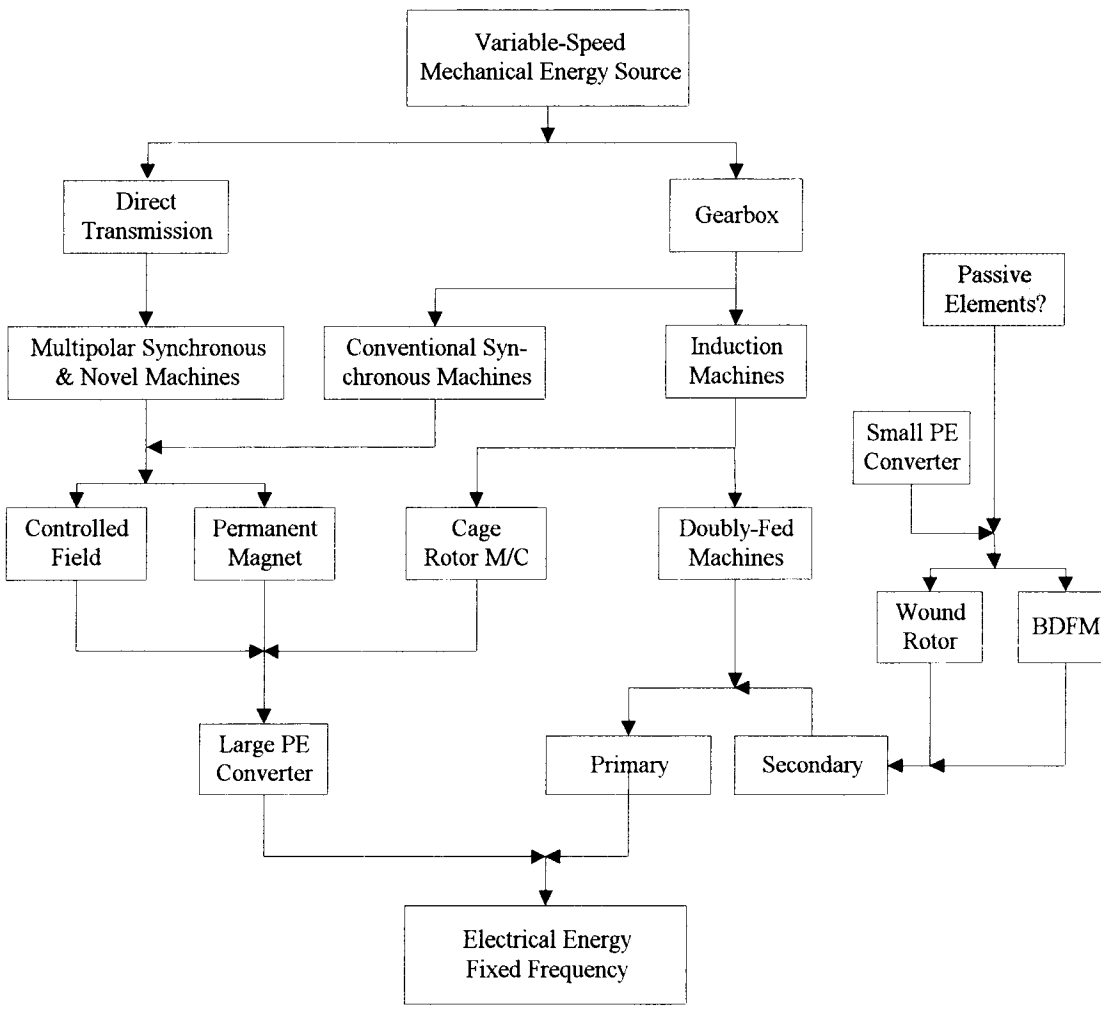

Figure 1.1 Mechanical to Electrical Energy Conversion Process

As is well known, additional rotor resistance extends the torque-speed characteristic of an induction motor or generator, but at the same time, worsens the efficiency characteristic of such a machine. However, connecting an inductor in parallel to such an additional rotor resistance leads to an efficiency increase, which can be explained with the frequency dependent inductive impedance. At low speed, just above the generator synchronous speed, the induced rotor frequency is low which results in a small inductor impedance tending to short circuit the resistor and therefore provides a system efficiency close to that of the generator alone. At the higher end of the speed operation range, the inductor impedance increases, passing the rotor current to the resistor branch, which determines the maximum of the operation speed. As is shown in this thesis, this operates satisfactorily in steady-state and dynamic conditions giving efficiencies that are close to corresponding power electronic control.

The practical tests were performed in the Motor System Resource Facility (MSRF) at Oregon State University (OSU), which has been the topic of many publications [10-12]. In late 1993 the MSRF was initiated by a consortium of the Electric Power Research Institute (EPRI), Bonneville Power Administration (BPA), the U.S. Department of Energy (DoE), and Pacific Gas and Electric Company (PG&E). The overall test bed configuration of the MSRF is illustrated in Fig. 1.2, and its technical data can be viewed in Appendix A.

The MSRF is an independent test laboratory that serves as a regional resource for conducting research and tests on electrical motors, generators, and adjustable speed drives (ASD) with ratings up to 300 hp. A regenerative, bi-directional vector controlled converter with an induction machine as dynamometer enables both motor and generator tests. The system is designed to operate in an energy re-circulation mode in which approximately 80 - 90 % of the demanded energy, depending on the device under test, is delivered back to the power grid. The MSRF also features a 600 A three-phase independent autotransfomer with a voltage range of 0 to 600 V/phase. The autotransformer phase voltage can be adjusted by both manual or three phase automatic operation over a driven gear system. This enables testing of single-phase machines besides multiphase machines in balanced, unbalanced, under-voltage or over-voltage conditions.

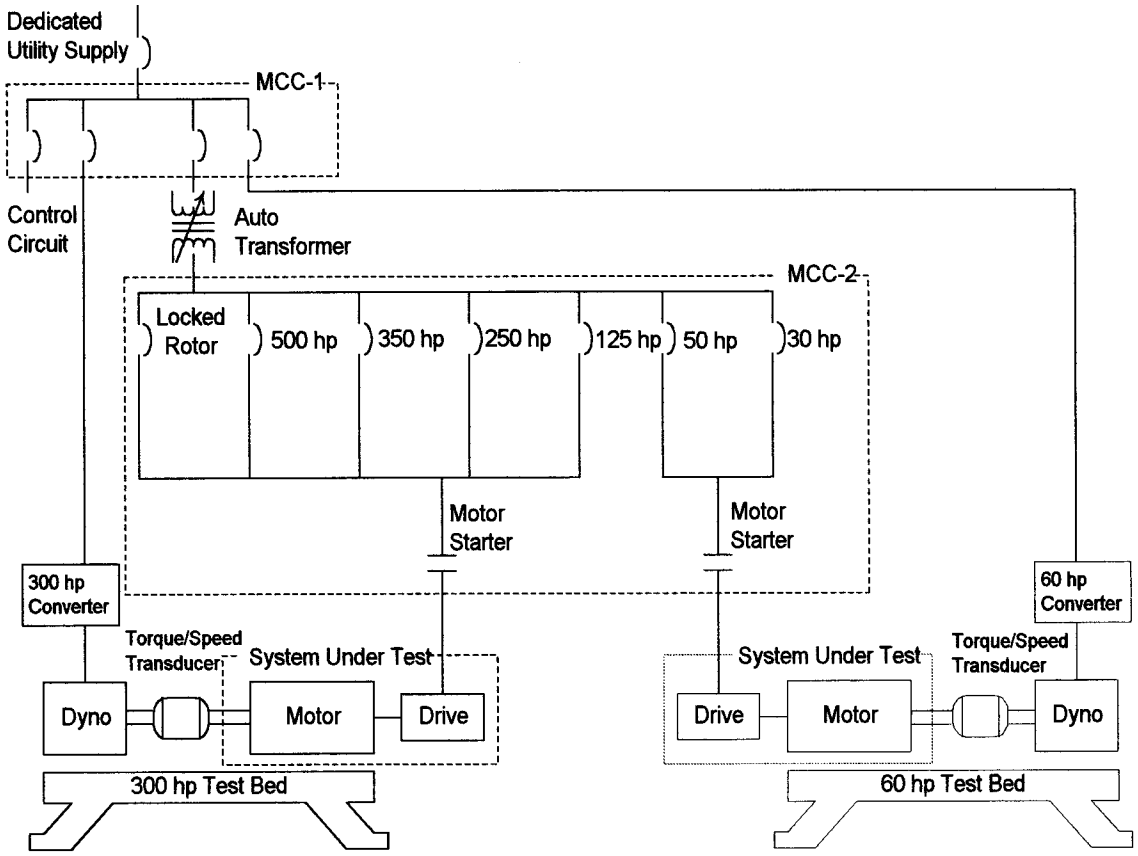

Figure 1.2 Motor System Resource Facility

In keeping with its goal of being a state-of-the-art electrical machine testing facility, the MSRF recently improved its steady state operation capability to one that also provides programmable dynamic operations. Some of the dynamic operations that it has acquired include the ability to apply a general, predefined torque and speed profile from a generalised polynomial function, a sine wave of torque or speed added to a constant speed offset, and a general purpose mode which allows the user to specify an atypical profile [13].

Again, the generators under test in this study have 80 kW and 186 kW ratings and their nameplate details are given in Appendix B. An operation speed range of 10 % and 20 % was chosen for the machines, implying an approximate rotor speed range of 1200 to 1300 rpm and 1200 to 1400 rpm for the 6-pole generators. Since the generator system

shows non-linear characteristics, iterative methods have been used to find proper passive/external elements assuring a rated power output at the higher end of the speed range while maintaining high efficiency. Under steady state operation a particular focus was made on the following machine characteristics to gather essential data for efficiency computation and future generator system design:

1) Output power
2) Torque
3) Power factor
4) Stator current
5) Rotor currents

Items of interest in the dynamic operation mode to receive sufficient information about stabilisation and power system issues were:

1) Connection to the grid at non-synchronous speed, to show non-ideal connection effects
2) Sudden decreases and increases in applied torque, to simulate wind gusts
3) Cyclic torque changes to demonstrate tower shadow effects.

Since balanced conditions are considered, the steady state simulations were performed on a per-phase equivalent circuit using the software tool Mathcad 6.0 [14]. For comparison to the practical tests, the steady state modelling also provides additional loss computations of each branch of the equivalent circuit.

The dynamic simulations were performed by a new numerical model using MATLAB/SIMULINK [15] as user software. This model is based on the dq induction machine model, which has been documented in many texts [16-19], using flux linkages as state variables. This model requires a repeated integration process using a Runge-Kutta technique. The final model obtained introduces the external inductor current as another state variable, while the simulation process is kept in the rotor reference frame. In Appendix C, the corresponding simulation source codes may be viewed.

2. THEORETICAL FUNDAMENTALS

2.1 Generator Requirements

The basic component of the proposed generator system is a wound-rotor induction machine. As is well documented, the torque-speed characteristics of this machine can be modified, to provide an extended speed operation range of the generator, by increasing in a controlled manner, the resistance to reactance ratio of the rotor circuit. Typically, the operation speed range of a high efficiency induction generator is approximately 1 %. To extend this to 10 % or 20 % requires substantial resistance to be added, which adversely affects the efficiency, particularly at the lower end of the speed range. Hence, modification of the connected resistance as a function of speed is essential. Historically this has been achieved by mechanical connections of the resistors, a high failure item in repeated cycling applications, and more recently by power electronics components, which require speed or frequency sensing and are prone to producing switching transients.

The passively controlled variable-speed generator system employs a parallel resistor-inductor combination connected over slip rings and brushes to the rotor. At the low-end of the speed operation range, just above the generator synchronous speed, the rotor frequency is low and the inductor tends to short-circuit the resistor giving a system efficiency close to that of the generator alone. At higher speeds the inductor impedance increases, diverting the rotor current into the resistive element and enabling the required extended speed range. As is analysed in this thesis, this operates satisfactorily and provides efficiencies that are close to corresponding power electronic controlled generator systems.

2.2 Passive Induction Generator Control

The use of adjustable resistors for the starting and speed control of wound rotor induction machines as shown in Fig. 2.1 [24] is documented in many texts [20-22], and is well known to be effective. An analysis of the rotor power of this system, with reasonable

approximations shows that the slip (s) at which peak torque of the motor occurs can be modified according to Equation 2.1

$$s = \pm \frac{R_T}{X_T} \tag{2.1}$$

in which

$$R_T = R_2' + R_{ex}' \tag{2.2}$$

and

$$X_T = X_1 + X_2' \tag{2.3}$$

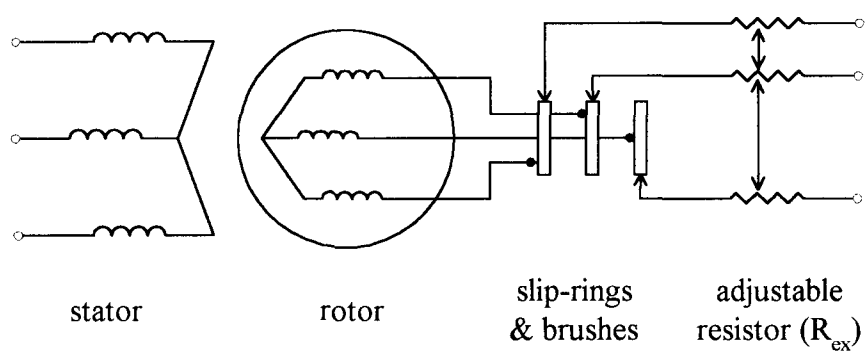

Figure 2.1 Wound-Rotor Induction Machine Contolled by Adjustable Resistance

Equation 2.1 is linear and can be solved analytically. If the machine parameters of X_1 and X'_2 (stator leakage and stator-referred rotor leakage reactances) and R'_2 (stator-referred rotor resistance) are known, a suitable value of R_{ex} can be determined to provide the required slip or speed operation range. However, modification of the machine performance in this way is inefficient, due to the increased losses in the external resistor, and the maintenance problems of mechanical switches used to modify the resistances can be considerable. Alternatively, the use of power electronic switching to modify the effective external resistance can lead to power quality issues.

The effect of a simple fixed resistor connected to the rotor circuit can be modified by the use of parallel reactive elements [7, 8, 23], as shown in the schematic of Fig. 2.2, in which the parallel reactive element can be capacitive, inductive, or both capacitive and inductive.

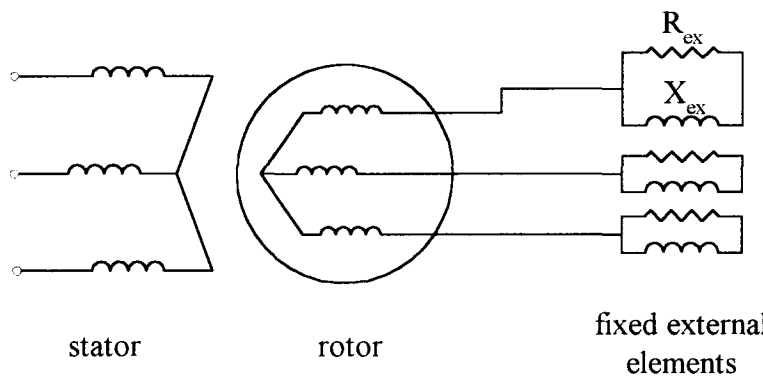

Figure 2.2 Wound-Rotor Induction Machine with Fixed Passive/External Elements

When referred to the stator, a per phase equivalent circuit of the form shown in Fig. 2.3 results in which R'_{eff} and X'_{eff} are the effective series components resulting from parallel elements in the slip-frequency rotor circuits. Those effective components can be expressed in case of parallel resistor and capacitor as

$$R'_{eff} = \frac{a^2 \cdot R_{ex} \cdot \frac{X_C^{\,2}}{s^3}}{R_{ex}^{\,2} + \left(\frac{X_C}{s}\right)^2} \tag{2.4}$$

$$X'_{eff} = \frac{-a^2 \cdot R_{ex}^{\,2} \cdot \frac{X_C}{s^2}}{R_{ex}^{\,2} + \left(\frac{X_C}{s}\right)^2} \tag{2.5}$$

and in case of parallel resistor and inductor as

$$R'_{eff} = \frac{a^2 \cdot s \cdot R_{ex} \cdot X_L{}^2}{R_{ex}{}^2 + (s \cdot X_L)^2} \tag{2.6}$$

$$X'_{eff} = \frac{a^2 \cdot R_{ex} \cdot X_L{}^2}{R_{ex}{}^2 + (s \cdot X_L)^2} \tag{2.7}$$

in which s is the fractional slip, a is the stator-rotor turns ratio, and X_C and X_L are the impedances of the capacitor and the inductor at line frequency, respectively.

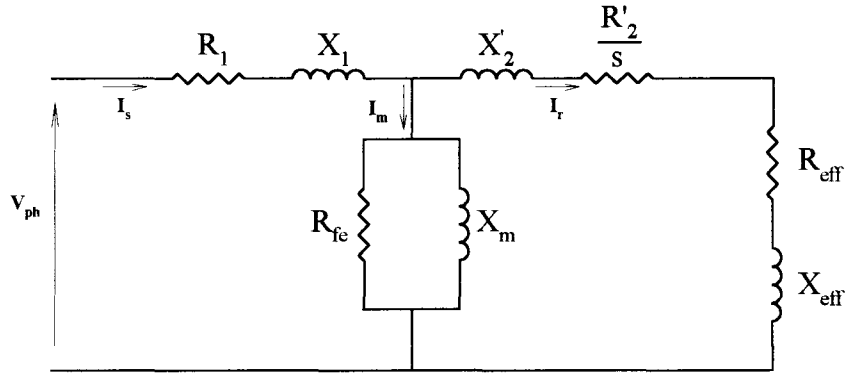

Figure 2.3 Equivalent Circuit of Wound Rotor Induction Machine with passive Control

Hence, it is evident that in both these cases the reactive elements are more effective in the determination of the effective resistance than is the external resistance itself. Also, as the slip plays a significant role in the effective resistive impedance, this can be employed to provide generator characteristics that match the ouput of variable speed energy sources.

For machine control by this technique, Equation 2.1 is still valid, but the total resistance and reactance values are extended to

$$R_T = R'_2 + R'_{eff} \tag{2.8}$$

and

$$X_T = X_1 + X_2' + X_{eff}' \tag{2.9}$$

Thus, in this case, Equation 2.1 becomes nonlinear with respect to the slip and cannot be used directly to devise a speed-control algorithm. However, suitable values for R_{ex}, X_C and X_L can be determined by iterative simulation. Initially a value for R_{ex} alone is determined by the generator reaching rated current at the upper speed limit.

It should be noted that in this thesis only the case of parallel resistor and inductor as external element combination was investigated, due to the unacceptable low efficiency of the resistor/capacitor combination for this specific wind turbine application [1]. Nevertheless, parallel capacitor or both capacitor and inductor may be suitable for other application areas of passive controlled generator systems.

3. PRACTICAL TESTS

3.1 Test Configuration

The practical tests were performed in the Motor System Resource Facility (MSRF) at OSU. Fig. 3.1 depicts the schematic of the test configuration. As is shown, the rotor speed ω_r can be controlled in both a steady-state and dynamic manner by means of a bi-directional adjustable speed drive (ASD) and an induction motor dynamometer. The torque and speed were measured with a Lebow 7540 torque-speed transducer, which was coupled between the dynamometer and the generator shaft. Because "energy capture" and cost of energy are significant parameters in the assessment of wind-turbine generator economic viability, very accurate efficiency data is needed. This requires precise electrical and mechanical calibrations.

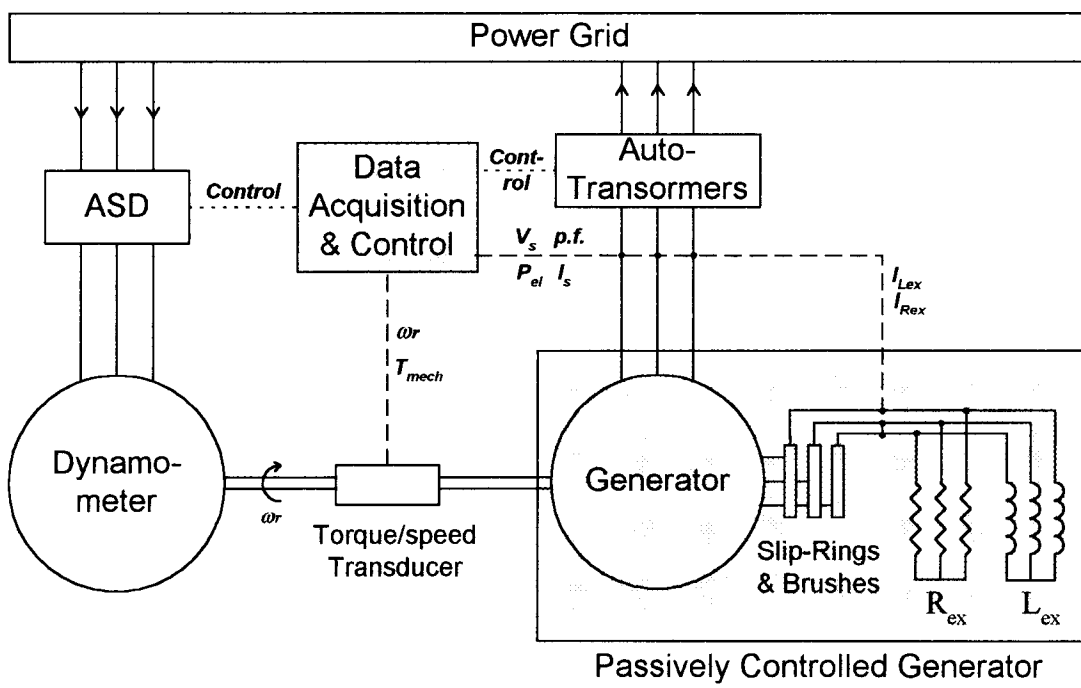

Figure 3.1 Test Set-up

Precise calibration of the torque-speed transducer assured a low speed and torque acquisition error of better than ± 0.5 %, which may be verified on the calibration example in Appendix A. Using a Voltech PM 3300 power analyser, the necessary generator output data, comprising electrical power output (P_{el}), stator current (I_s), rotor currents (I_{rex}, I_{Lex}), stator voltage (V_s), and power factor (p.f.) were collected. The Y-connected passive/external R-L elements were linked to the rotor windings via slip-rings.

All control schemes for the ASD and the 3-phase autotransformer are interfaced over a GPIB serial link to a personal computer (PC). A DOS-based as well as a 'C'-based, communication program implements the control process from the user's side [13].

3.2 Steady-State Tests

In order to receive valuable steady-state information of the new, passive-controlled generator concept, two systems, with respective ratings of 80 kW and 186 kW, were tested. For each generator system different external elements were computed to provide in case of the 80 kW machine a speed operation range of 1200 to 1300 r/min and for the 186 kW machine a range of 1200 to 1400 r/min. The measured data of the controlled generator was compared to the measured data obtained by the generator itself.

3.2.1 Generator System of 80 kW Rating

The 80 kW experiment was carried out on a slip ring wound-rotor induction machine whose machine parameters are shown in Table 3.1. The parameters are based on a per-phase Y-connected equivalent circuit. Further nameplate and manufacture data are given in Appendix B. Since the system shows non-linear characteristics, iterative methods have to be used to find the appropriate passive/external elements. To provide for this application a speed range of 1200 – 1300 r/min while maintaining highest possible efficiency, the passive elements were computed to the values shown in Table 3.1.

hp = 107 (80 kW)	r/min = 1212
Volts = 480 V	I = 114 A
poles = 6	a = 2.5 (rotor : stator turn ratio)
J = 3.5 kg·m^2	R_1 = 0.022 Ω
X_1 = 0.12 Ω	R_{fe} = 466 Ω
X_m = 8.47 Ω	R'_2 = 0.045 Ω
X'_2 = 0.603 Ω	R_{ex} = 1.07 Ω
L_{ex} = 0.37 H	R_{L_ex} = 0.57 Ω

Table 3.1 Generator System Parameters (80 kW)

3.2.1.1 Test Results and Efficiency

Table 3.2 gives the experimental results in case of passive speed controlling and, in comparison, Table 3.3 shows the results in case the rotor windings are shorted (fixed-speed). For each test, the maximum power (80 kW) and current (114 A) ratings of the generator were targeted. As seen, the efficiency of the passive controlled configuration, calculated by using Equation 3.1, reaches a maximum of 91.2 %, which is 3.2 % lower than the maximum efficiency (94.4 %) of the fixed-speed application.

$$\eta = \frac{P_{out}}{P_{in}} = \frac{P_{out}}{\omega \cdot T_{mech}} \tag{3.1}$$

where

$$\omega = 2 \cdot \pi \cdot \text{speed} \tag{3.2}$$

This reduction, caused by the external elements as shown later in Section 3.2.1.2, is still comparable to that obtained with adjustable frequency control of similarly rated induction machine as depicted later in Section 3.2.4. Observing the external rotor currents I_{Rex} and I_{Lex} makes the effect of the frequency dependent external impedance evident. At low speed, the inductor impedance is low, enabling the current to flow predominantly through the inductor and therefore providing a generator system efficiency close to that obtained

by the generator itself. In contrast, as the rotor speed increases, so the inductor impedance increases, passing the rotor current to the external resistor, which determines the upper operation speed range, and hence, forcing the inductor current to become limited. The reduced power factor can be attributed to the additional inductance of the external inductor, which decreases the resistance to impedance ratio R:Z of the system. Thus, the effect of increasing the speed range from 1.6 % (rotor shorted) to 8.3 % (R/L controlled) is given in Tables 3.2 and 3.3.

Speed (r/min)	Efficiency (%)	Torque (Nm)	P_{out} (kW)	I_s (A)	p.f.	I_{Rex} (A)	I_{Lex} (A)
1202	64.3	31.0	2.51	33.3	0.089	0.9	1.4
1203	73.2	41.0	3.78	34.1	0.131	1.0	1.5
1205	80.7	56.0	5.70	35.5	0.191	2.0	2.0
1210	86.3	88.5	9.68	38.9	0.297	4.0	3.2
1215	89.2	117.5	13.33	42.0	0.379	6.0	3.3
1225	90.5	185.2	21.50	48.2	0.532	9.5	3.3
1250	91.2	343.0	40.97	67.3	0.728	20.0	3.3
1275	89.4	505.0	60.30	89.9	0.803	30.5	3.4
1300	87.9	662.0	79.21	114.1	0.829	40.0	3.4

Table 3.2 Tested Results of R/L Controlled Generator System (80 kW)

Speed (r/min)	Efficiency (%)	Torque (Nm)	P_{out} (kW)	I_s (A)	p.f.
1201	79.9	45	4.52	33.1	0.164
1202	85.3	74	7.95	34.25	0.278
1203	89.8	110	12.45	36.6	0.407
1204	91.2	133.0	15.31	38.7	0.474
1205	92.8	164.0	19.20	41.5	0.559
1210	94.4	356.1	42.61	64.9	0.784
1213	94.4	465.0	55.78	80.1	0.827
1220	93.7	676.0	80.90	112.3	0.859

Table 3.3 Tested Results of Rotor Shorted Generator System (80 kW)

3.2.1.2 Loss Segregation

To investigate the power dissipation in the generator and the external elements, a segregation of the losses is summarised in Table 3.4. The loss computation is based on an approximated per-phase equivalent circuit as shown in Fig 3.2, and the losses of each resistive element are calculated by Equations 3.3 - 3.7.

$$P_{R1} = 3 \cdot I_s^{\,2} \cdot R_1 \tag{3.3}$$

$$P_{Rfe} = 3 \cdot \frac{V_{ph}^{\,2}}{R_{fe}} \tag{3.4}$$

$$P_{R2} = 3 \cdot \left(I_{Rex}^{\,2} + I_{Lex}^{\,2}\right) \cdot R_2' \cdot a^2 \tag{3.5}$$

$$P_{Rex} = 3 \cdot I_{Rex}^{\,2} \cdot R_{ex} \tag{3.6}$$

$$P_{Lex} = 3 \cdot I_{Lex}^{\,2} \cdot R_{Lex} \tag{3.7}$$

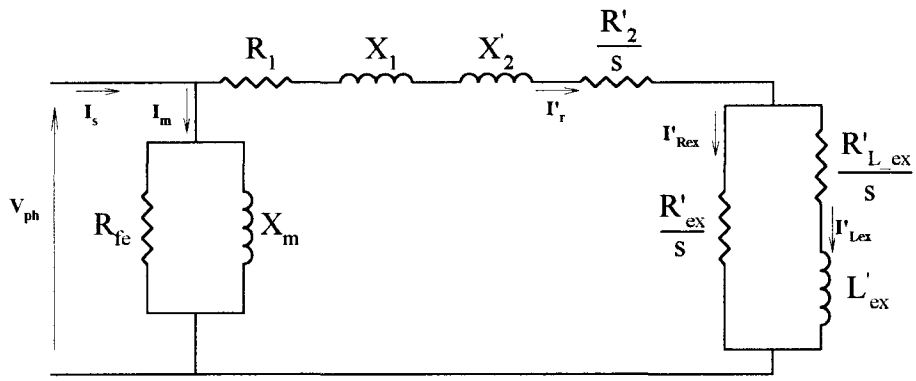

Figure 3.2 Approximate Per-phase Equivalent Circuit

Speed (r/min)	P_{R1} (W)	P_{Rfe} (W)	P_{R2} (W)	P_{Rex} (W)	P_{Lex} (W)
1202	72	494	2	2	3
1203	77	494	3	3	4
1205	83	494	7	13	7
1210	100	494	22	53	18
1215	116	494	40	119	19
1225	153	494	85	298	19
1250	299	494	347	1320	19
1275	533	494	795	3070	20
1300	860	494	1360	5280	20

Table 3.4 Tested Losses (80 kW)

As expected, the iron losses predominate at lower speed because of the high resistive rotor branch caused by the small slip (s). At higher speed, the most power dissipates in the external resistor, which is shown to be the main reason for the efficiency reduction from 94.4 % to 91.2 %, determined in Section 3.2.1.1. Adequate cooling considerations should be undertaken to prevent damaging the external resistor. P_{r1} and P_{r2} does not show abnormal values and P_{lex} can be neglected.

3.2.2 Generator System of 186 kW Rating

The same type of machine was used for the 186 kW generator system test, whose parameters are listed in Table 3.5, which are also based on a per-phase Y-connected equivalent circuit. Also for this machine, further nameplate and manufacturer data may be viewed in Appendix B. To operate in the speed range of 1200 – 1400 r/min while maintaining highest efficiency, the passive elements were calculated to values shown in Table 3.5

hp = 250 (186 kW)	r/min = 1180 (motoring)
Volts = 460 V	I = 290 A
poles = 6	a = 2.01 (rotor : stator turn ratio)
$J = 9\ kg{\cdot}m^2$	$R_1 = 0.0095\ \Omega$
$X_1 = 0.0893\ \Omega$	$R_{fe} = 105.429\ \Omega$
$X_m = 2.667\ \Omega$	$R'_2 = 0.0133\ \Omega$
$X'_2 = 0.0848\ \Omega$	$R_{ex} = 0.595\ \Omega$
$L_{ex} = 0.034$ H	$R_{L\_ex} = 0.19\ \Omega$

Table 3.5 Generator System Parameters (186 kW)

3.2.2.1 Test Results

The test results for both R/L controlled and rotor shorted operation are given in Tables 3.6 and 3.7, respectively. The maximum capacity of the torque/speed transducer is 1150 Nm, which limits the speed range and therefore bounded the maximum measurable output power to 71% of the generator. It is evident that the maximum efficiency of 88.3 %, in comparison to the 91.2% of the 80 kW application is mainly caused by the higher external resistor required to enable the 20 % speed range. This statement is proven in the next section, where a breakdown of the losses is provided. Another difference to the 80 kW application shows the smaller I_{Rex}: I_{Lex} ratio at higher speed, which is due to the low

inductance L_{ex} and hence results in a relative low coil impedance in the upper speed range. Otherwise, similar effects and trends were observed as in the 80 kW experiment.

Speed (r/min)	Efficiency (%)	Torque (Nm)	P_{out} (kW)	I_s (A)	p.f.	I_{Rex} (A)	I_{Lex} (A)
1205	77.6	150	14.70	99.8	0.184	2.9	4.7
1210	84.5	245	26.23	111.0	0.294	5.8	9.3
1215	87.2	323	35.82	125.2	0.358	7.9	14.5
1220	88.0	368	41.36	135.5	0.382	10.8	20.0
1225	88.3	400	45.3	143.3	0.396	14.0	23.0
1250	87.9	544	62.58	169.1	0.464	30	29.0
1275	87.2	702	81.70	189.0	0.542	46.2	30.5
1300	86.2	875	102.74	210.9	0.612	62.9	31.1
1325	85.0	1050	123.8	234.2	0.664	79.0	31.5
1335	84.4	1125	132.7	244.9	0.680	86.2	31.7

Table 3.6 Tested Results of R/L Controlled Generator System (186 kW)

Speed (r/min)	Efficiency (%)	Torque (Nm)	P_{out} (kW)	I_s (A)	p.f.
1201	39.0	51	2.5	94.1	0.021
1202	79.9	175	17.6	97.4	0.212
1203	85.9	280	30.3	103.6	0.371
1204	91.2	455	52.3	118.7	0.552
1205	92.2	583	67.8	132.7	0.642
1207	93.0	765	89.9	155.4	0.724
1209	93.2	900	106.2	174.0	0.762
1211	94.1	1110	132.4	205.0	0.810

Table 3.7 Tested Results of Rotor Shorted Generator System (186 kW)

3.2.2.2 Loss Segregation

The same algorithm and equivalent circuit as in Chapter 3.2.2.1 was used for this loss segregation. In comparison to the 80 kW system, the iron losses of this machine are more dominant, while the external coil losses already reach a considerable value of 13.3 kW at 1335 r/min. In Chapter 3.2.3.3 the loss curves are extrapolated to project the loss distribution up to 1400 r/min. Another difference can be observed in the smaller P_{rex}:P_{Lex} ratio due to the lower I_{Rex}:I_{Lex} ratio. Otherwise, similar findings were obtained as in the 80 kW test as seen in Table 3.8.

Speed (r/min)	P_{R1} (W)	P_{Rfe} (W)	P_{R2} (W)	P_{Rex} (W)	P_{Lex} (W)
1205	284	2007	5	40	5
1210	351	2007	19	60	49
1215	447	2007	44	111	120
1220	523	2007	83	208	228
1225	585	2007	117	350	301
1250	815	2007	280	1607	479
1275	1018	2007	493	3810	530
1300	1268	2007	793	7062	551
1325	1563	2007	1165	11140	566
1335	1709	2007	1385	13263	572

Table 3.8 Tested Losses (186 kW)

3.2.3 Graphical Representation of Test Results

3.2.3.1 Efficiency and Power Factor

In Figs. 3.3 and 3.4, the efficiency and power factor characteristics, of both the passively-speed controlled generator system and the generator itself, are shown. They illustrate the efficiency and power factor behaviour versus normalised output power for the 80 kW and 186 kW machines, respectively. In the case of the 186 kW generator, the efficiency and power factor curves had to be extrapolated due to the limited torque transducer capability, which reaches its maximum at about 70 % of the output power. As depicted, both machines show a characteristic of relevance to wind turbine applications with a substantial efficiency over a wide speed range. In both illustrations, a deviation between the controlled and non-controlled performance appears after about 10 % of the maximum power output, which is assumed, due to the bypass effect of the external resistor through the inductor at low speeds and rotor frequencies. In consequence, the lower per unit external resistor (R_{ex}), used for the 80 kW system obtains better efficiency and the difference between the controlled and non-controlled power factor is smaller. Hence, depending on the application, still higher efficiencies may be reached by decreasing the external resistor (R_{ex}), if smaller speed ranges are needed.

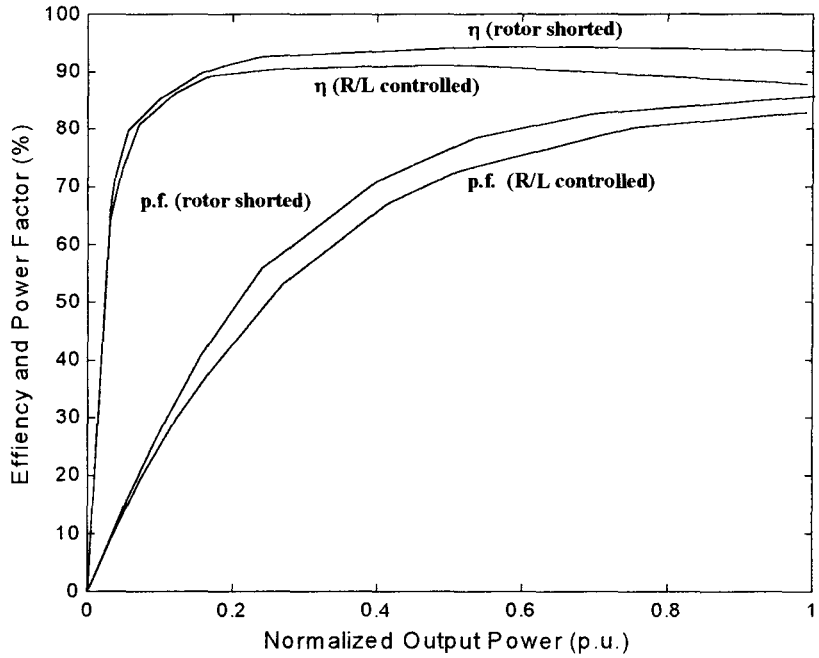

Figure 3.3 Tested Efficiency and Power Factor (80 kW)

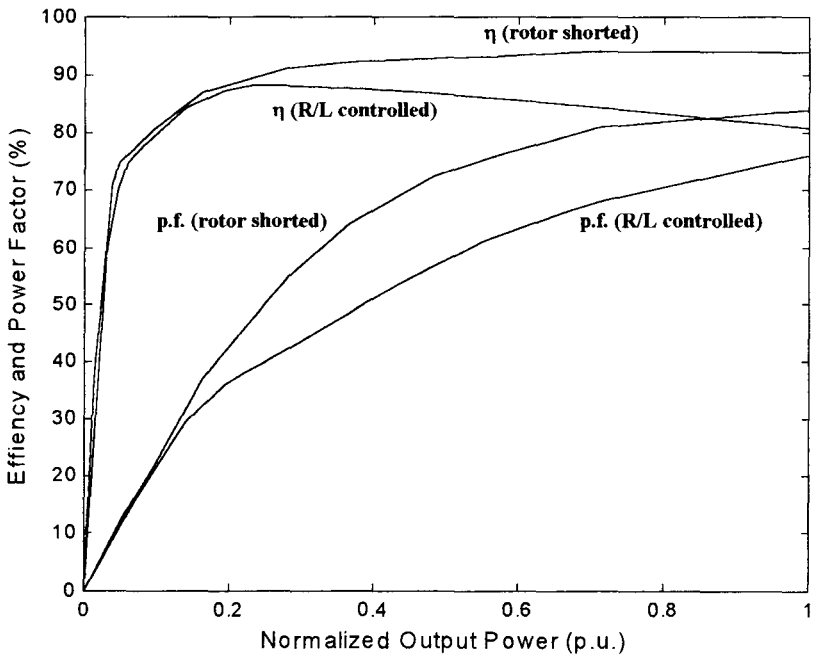

Figure 3.4 Tested Efficiency and Power Factor (186 kW)

3.2.3.2 Rotor Currents

Fig. 3.5 depicts the external rotor currents I_{Rex} and I_{Lex} versus speed of each generator system. Both external inductor currents show the same limiting effect caused by the constant external resistor and the frequency dependent external inductor; the current ratios I_{rex}:I_{Lex} behave reciprocal as the impedance ratio R_{ex}:Z_{Lex}. The different I_{Rex}: I_{Lex} ratio of the two generator systems, finds its explanation in the low inductance (L_{ex}), used for the 186 kW application.

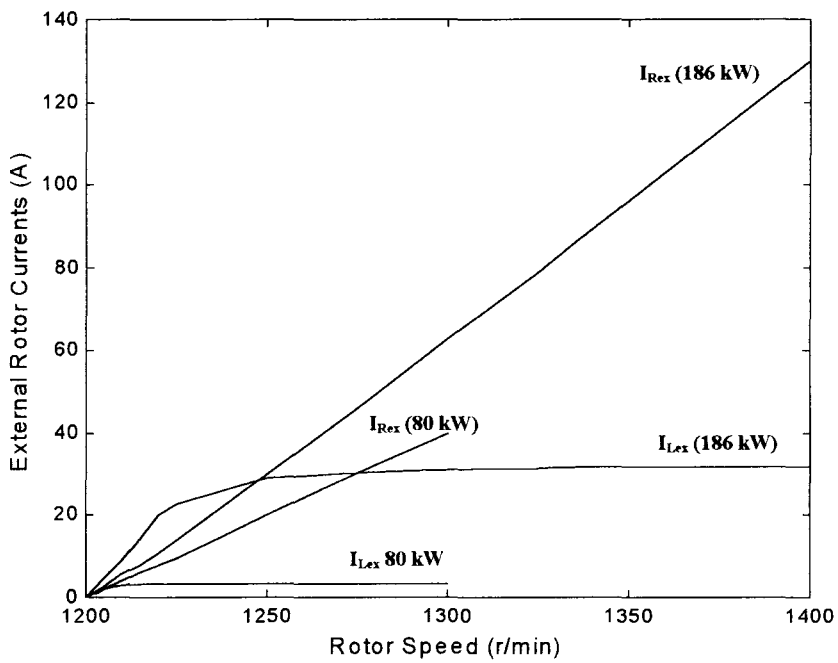

Figure 3.5 Tested External Rotor Currents (80 and 186 kW)

3.2.3.3 Losses

Figs. 3.6 and 3.7 represent the losses of the 80 kW and 186 kW passively controlled generator systems, respectively. In each diagram, the dominance of the external resistor losses (R_{ex}) is evident. Hence, cooling schemes should assure appropriate heat dissipation to avoid damage to those resistors.

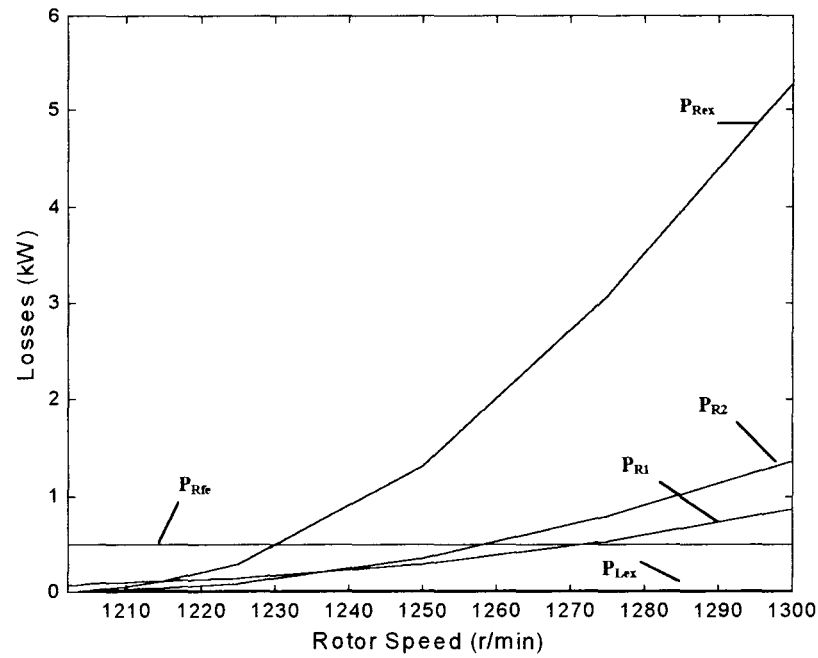

Figure 3.6 Tested Losses (80 kW)

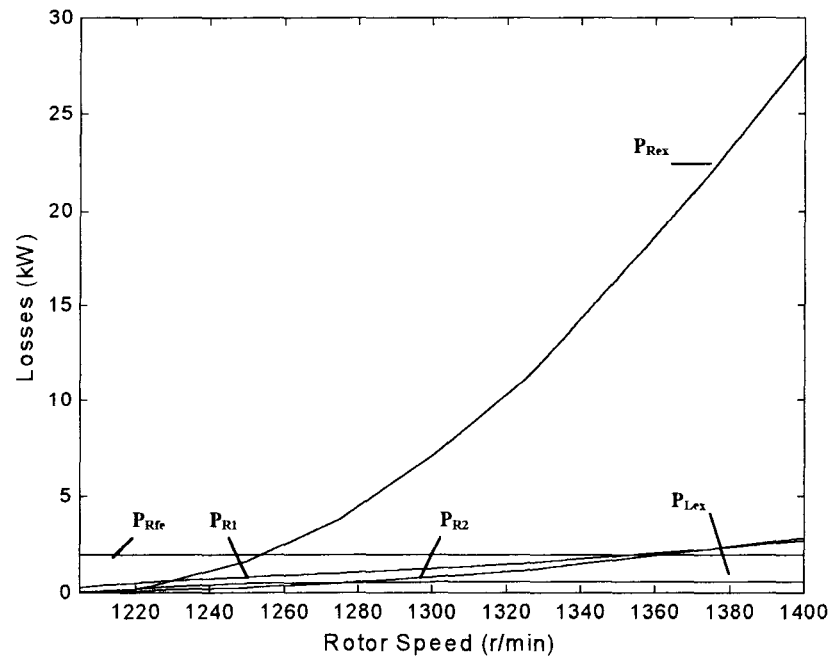

Figure 3.7 Tested Losses (186 kW)

In contrast, the coil losses (P_{Lex}) are found to be negligible, especially for the 80 kW application they are hardly visible in the graph. The typical constancy of the iron losses (P_{Rfe}), of the induction machines can be seen, which indicates their relative importance during low speed operation. Furthermore, the stator and rotor losses (P_{R1} and P_{R2}) behave in a similar way, in accordance with the general induction machine characteristics.

3.2.4 Comparison between Passive and Power Electronic Generator System

In order to compare the efficiency characteristic of the passively controlled variable-speed generator system analysed in this thesis to one which is controlled by power electronics, the efficiencies of the 80 kW and 186 kW units and of a power electronic controlled generator system is illustrated in Fig. 3.8. It was beyond the scope of this thesis to obtain data for the power electronically controlled system, consequently some previously available data [25] for a 275 kW doubly-fed wound-rotor induction machine system were used for comparison. As shown in Fig. 3.8, both of the passively controlled generator schemes show comparable efficiencies, which are better than the power electronic controlled system at lower speed operation. The range of speed required also affects this comparison, as has been shown previously.

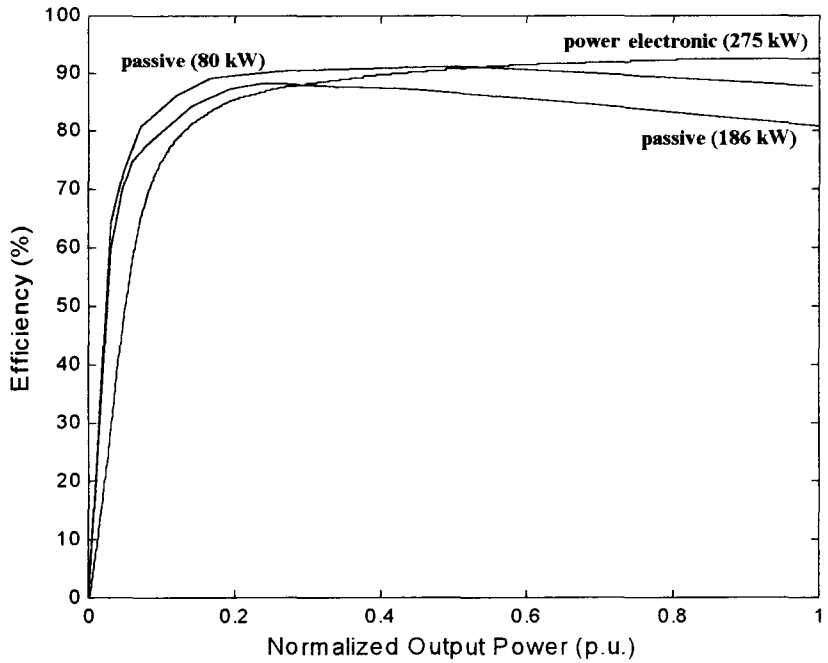

Figure 3.8 Efficiency Comparison

3.3 Dynamic Tests

During dynamic testing, the mechanical torque (T_{mech}), the stator current (I_s), and the rotor speed (n_r) were of interest. The data acquisition was carried out with a Tektronix TDS 460 A oscilloscope, which received its torque and speed signals directly from the Lebow 7540 torque/speed transducer, while the current was measured over a Fluke 80 I-1000s current probe. To receive sufficient information about stabilisation and power system issues a focus was made on three dynamic experiments:

1) Connection to the grid at non-synchronous speed, to show non-ideal connection effects
2) Sudden decreases and increases in applied torque - both positive and negative, to simulate wind gusts
3) Cyclic torque changes, to demonstrate tower shadow effects.

3.3.1 Generator System of 80 kW Rating

3.3.1.1 Non-Synchronous Connection

Fig. 3.9 illustrates the system response from a direct connection to the supply of the generator operating at 1225 r/min to show non-ideal connection effects. The transients verify adequate damping of the system; neither the mechanical torque (T_{mech}) nor the stator current (I_s) reach serious peak values. An initial torque peak of 675 Nm oscillates down to a steady state of 185 Nm, with a starting frequency of approximately 15 Hz determined by the inertia and mechanical damping characteristics. The inrush current peak of 800 A reduces within 0.1 s to a steady state peak of 70 A. It should be noted that the first current and torque peak depends on the momentary point-on-wave value of the supply voltage at the time of connection. Consequently, higher and lower torque and current peaks may occur.

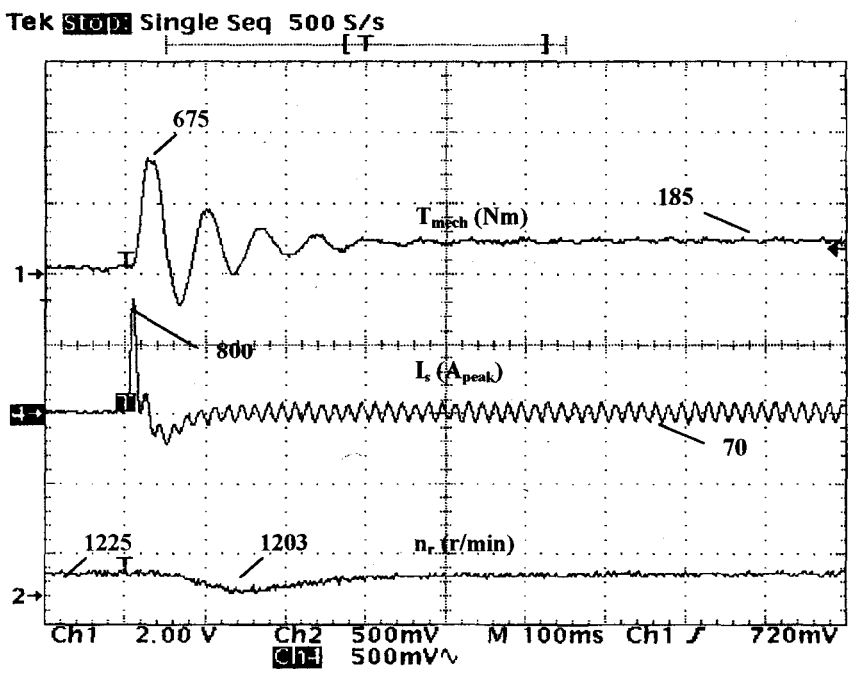

Figure 3.9 Tested Connection to Grid at Non-synchronous Speed (80 kW)

Nevertheless, later in this thesis, the dynamic simulations prove that those values are already in the maximum region of the initial peaks. The speed drop to 1203 r/min finds its explanation in the dynamometer, which is not able to maintain a constant speed due to the severe change of torque within a short period of time. The delay of about 0.06 s results from the rotor inertia of the generator and dynamometer.

3.3.1.2 Responses to Sudden Torque Change

Fig. 3.10 indicates the system reaction to sudden torque changes that may be caused by wind gusts. Here it is seen that the system responds in a "soft" manner and should not cause any problems in practice. Starting with a constant speed of 1225 r/min, a mechanical torque of 345 Nm, and a generated current of 100 A peak, the dynamometer forces the generator to change to a new steady-state condition of a speed of 1225 r/min, a torque of 185 Nm, and a generator current of 70 A peak. After about 1.5 s the system undergoes another, more severe, change to the final steady-states of 505 Nm, 130 A peak,

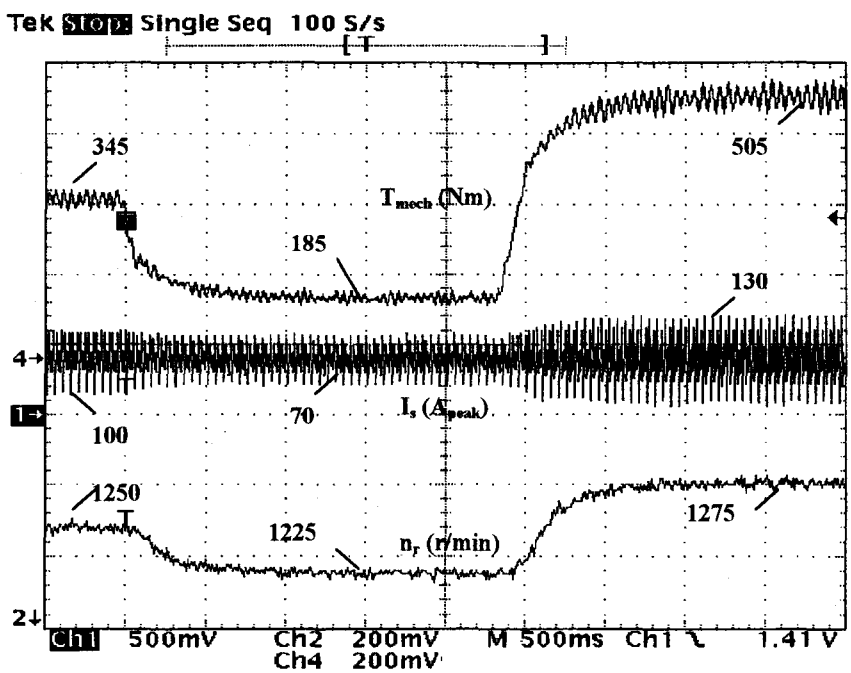

Figure 3.10 Tested Sudden Change of Torque (80 kW)

and 1275 r/min. The response time of about 1.5 s indicates that the passively controlled generator system reaches new steady-state conditions quickly without showing any considerable disturbances.

3.3.1.2 Responses to Cyclic Torque Variations

Fig. 3.11 illustrates a practical demonstration of tower shadow effects. This is simulated by applying a sinusoidal speed signal of ± 20 r/min on top of a constant speed of 1240 r/min. However, according to the inertia of the generator and dynamometer, an actual speed oscillation from 1228 to 1252 r/min is realised. The corresponding mechanical torque pulsates between 190 and 340 Nm, while the generator current gives maximums of 90 and 70 A peak. No difficulties are seen with this behaviour as the generator tracks the input in a stable matter.

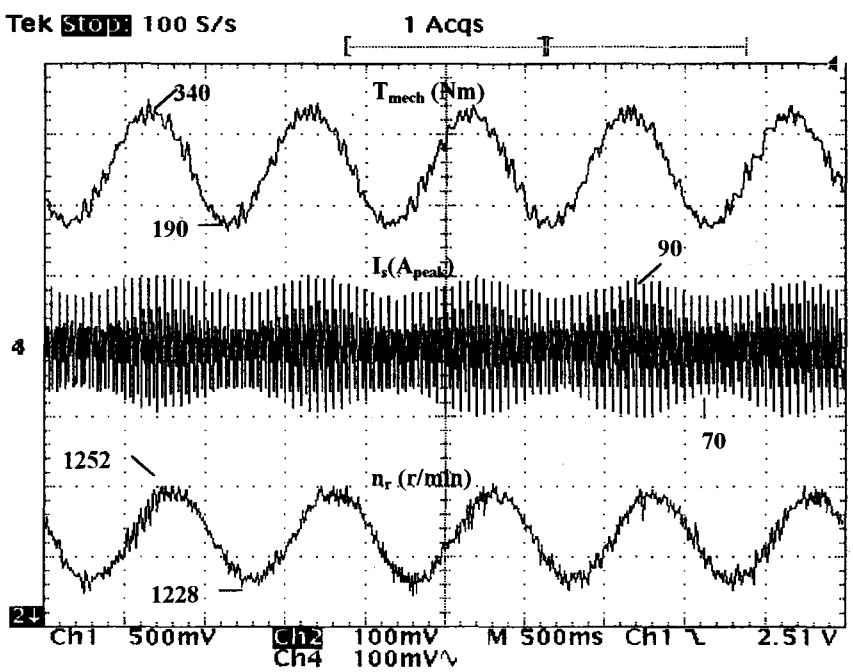

Figure 3.11 Tested Cyclic Torque Change (80 kW)

3.3.2 Generator System of 186 kW Rating

Also for the 186 kW system no severe dynamic responses were observed, as may be verified in Figs. 3.12 to 3.14. Neither in the case of non-synchronous connection to the power grid (Fig. 3.12), nor for the other two input profiles sudden change of torque (Fig. 3.13), and cyclic torque change (Fig. 3.14) unreasonable system transients occur. All characteristic values are directly marked in the diagrams. As expected, higher, but still acceptable transients can be observed in comparison to the 80 kW unit, in consequence of the larger rating. Nevertheless, it should be assured that safety equipment such as circuit breakers are suitably designed to carry those initial current peaks.

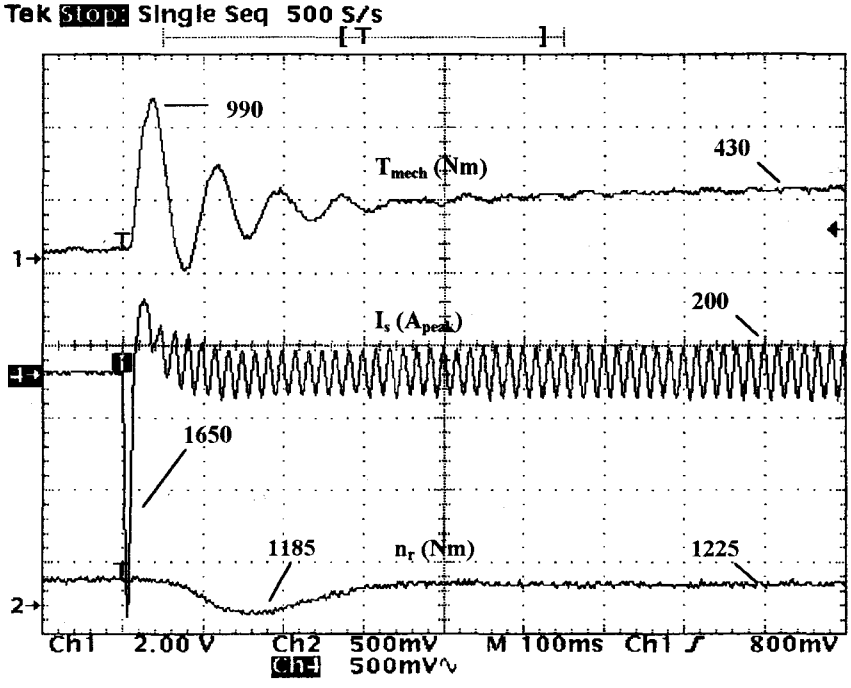

Figure 3.12 Tested Connection to Grid at Non-synchronous Speed (186 kW)

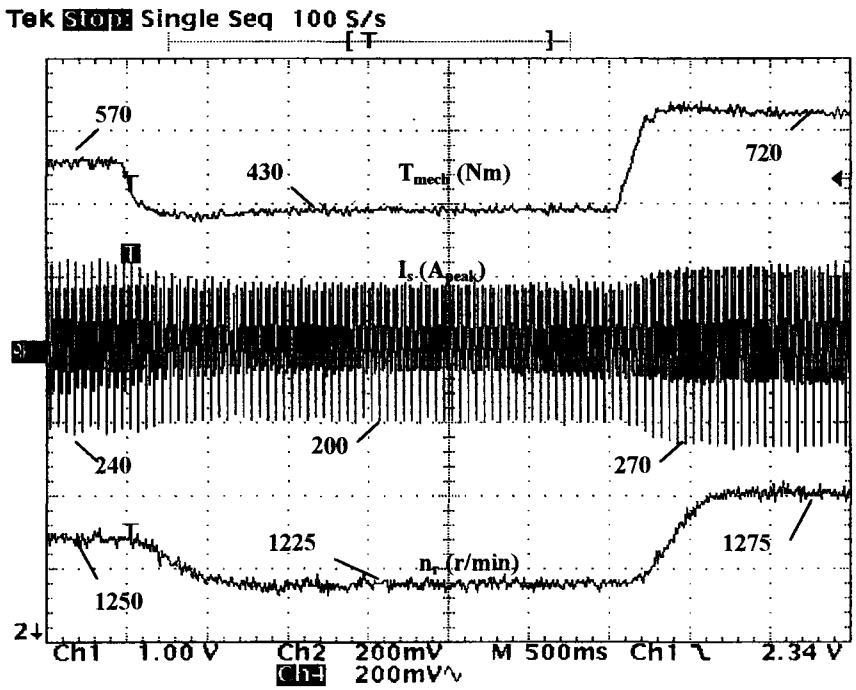

Figure 3.13 Tested Sudden Change of Torque (186 kW)

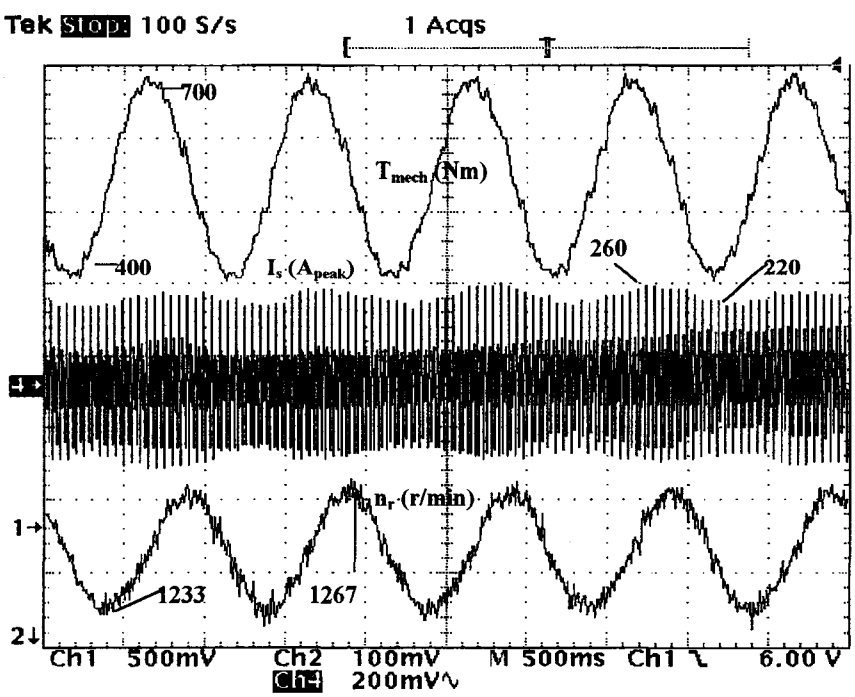

Figure 3.14 Tested Cyclic Torque Change (186 kW)

4. SIMULATIONS

4.1 Steady State Simulations

The steady state simulations were performed with Mathcad 6.0 as user software. Since balanced conditions have been considered, the simulations have been based on a typical single-phase equivalent circuit of an induction machine having assumed Y-connected windings. Hence, the final equivalent circuit, as shown in Fig. 4.1, includes the effective parallel connected external elements, which are linked to the rotor branch. The resistor R'_{L_ex} represents the stator referred value of winding resistance of the external inductor (L_{ex}). The current arrows of Fig. 4.1 are drawn in the typical motor mode, however, during generation the current actually flows in the opposite direction, resulting in a negative stator current (I_s). In order to obtain characteristic steady state data of the passively controlled generator system such as efficiency, output power, torque, power factor, stator current, rotor currents, and losses the following equation algorithm, starting by Equation (4.1), has been used

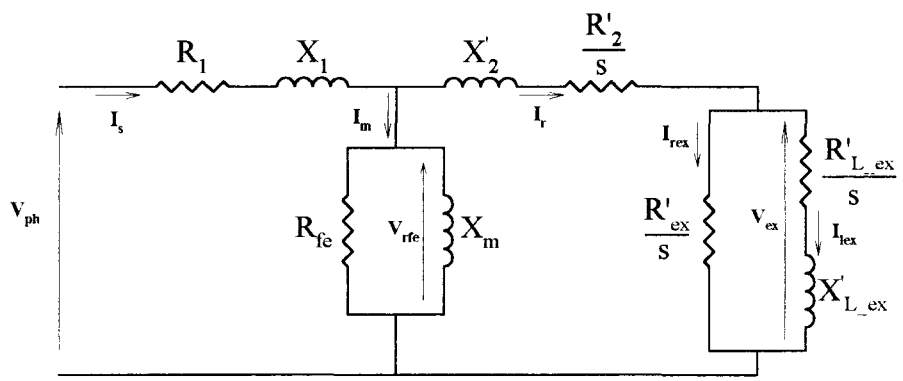

Figure 4.1 Per-phase Equivalent Circuit

With the calculation of the total impedance (Z_t) using Equation (4.1)

$$Z_t = \frac{\left\{ \frac{\left(\frac{R'_{L\_ex}}{s} + jX'_{L\_ex} \right) \frac{R'_{ex}}{s}}{\frac{R'_{L\_ex} + R_{'ex}}{s} + jX'_{ex}} + \frac{R'_2}{s} + jX'_2 \right\} \cdot \left(\frac{R_{fe} \cdot jX_m}{R_{fe} + jX_m} \right)}{\left\{ \frac{\left(\frac{R'_{L\_ex}}{s} + jX'_{L\_ex} \right) \frac{R'_{ex}}{s}}{\frac{R'_{L\_ex} + R_{'ex}}{s} + jX'_{ex}} + \frac{R'_2}{s} + jX'_2 \right\} + \left(\frac{R_{fe} \cdot jX_m}{R_{fe} + jX_m} \right)} + R_1 + jX_1 \quad (4.1)$$

the power factor (p.f.)

$$p.f. = \cos(\gamma) = \frac{\text{real}\{Z_t\}}{|Z_t|} \quad (4.2)$$

and the stator current (I_s) can be computed, which is actually negative due to the negative slip (generator mode).

$$I_s = \frac{V_{ph}}{Z_t} \quad (4.3)$$

Therefore the electrical output power (P_{out}), flowing into the power grid results as

$$P_{out} = 3 \cdot V_{ph} \cdot I_s \cdot \cos(\gamma) \quad (4.4)$$

In order to receive the torque and the efficiency of the passively controlled generator system, first, the losses in each resistive element of the equivalent circuit have to be calculated. The stator winding losses (P_{R1}) are simply derived by

$$P_{R1} = 3 \cdot I_s^2 \cdot R_1 \quad (4.5)$$

and the iron losses (P_{Rfe}) may be derived via the voltage

$$V_{Rfe} = V_{ph} - I_s \cdot (R_1 + jX_1) \quad (4.6)$$

which leads to

$$P_{Rfe} = 3 \cdot \frac{V_{Rfe}^2}{R_{fe}} \quad (4.7)$$

Using the stator referred rotor current (I'_r) and R'_2, the rotor winding losses (P_{R2}) may be computed as

$$P_{R2} = 3 \cdot I_r^{'2} \cdot R_2^{'} \tag{4.8}$$

where $I_r^{'}$ is larger than I_s, because of the generator mode.

$$I_r^{'} = I_s - \frac{V_{Rfe}}{\frac{R_{fe} \cdot jX_M}{R_{fe} + jX_M}} \tag{4.9}$$

The external element voltage (V'_{ex}) may be expressed as

$$V_{ex}^{'} = I_r^{'} \cdot \frac{\left(\frac{R_{L\_ex}^{'}}{s} + jX_{L\_ex}^{'} \right) \frac{R_{ex}^{'}}{s}}{\frac{R_{L\_ex}^{'} + R_{,ex}}{s} + jX_{ex}^{'}} \tag{4.10}$$

with which the external resistor losses (P_{Rex}) may be calculated as

$$P_{Rex} = 3 \cdot \frac{V_{ex}^{'2}}{R_{ex}^{'}} \tag{4.11}$$

The external current (I'_{Lex}) flowing through the external inductor may be given by

$$I_{Lex}^{'} = I_r^{'} - I_{Rex}^{'} \tag{4.12}$$

where

$$I_{Rex}^{'} = \frac{V_{ex}^{'}}{R_{ex}^{'}} \tag{4.13}$$

Thus, the external losses (P'_{Lex}) through the dc resistance of the external inductor results in

$$P_{Lex} = 3 \cdot I_{Lex}^{'2} \cdot R_{L\_ex} \tag{4.14}$$

Hence, knowing all losses of each resistive element, enables the calculation of the mechanical torque (T_{mech}) and the efficiency η of the generator system. The input power (P_{in}) is the mechanical power which applies on the rotor shaft and which can be expressed

by the sum of all losses of the equivalent circuit plus the friction (P_{fr}) of the generator. With the torque, the rotor speed (ω_r), and Equation (4.16) the friction losses may be derived and thus

$$P_{in} = P_{R1} + P_{Rfe} + P_{R2} + P_{Rex} + P_{Lex} + P_{fr} \tag{4.15}$$

Therefore the torque (T_{mech}) is

$$T_{mech} = \frac{P_{in}}{\omega_r} \tag{4.16}$$

Finally, the efficiency (η) as a function of slip can be derived as

$$\eta = \frac{P_{out}}{P_{in}} \tag{4.17}$$

In this investigation the friction torque has been measured for both generator units and came to a mean of T_{mech} = 5 Nm for the 80 kW generator, and T_{mech} = 15.5 Nm for the 186 kW unit.

4.1.1 Simulation Results

4.1.1.1 Generator System of 80 kW Rating

Tables 4.1 to 4.3 show the simulated results for the 80 kW unit. As seen, the simulated values correspond well to the experimental ones and indicate correct simulations. In general, at higher speeds, the modelled results deviate from the test results with an error of ± 3 %. Possible causes of these deviations may be found by unbalanced conditions of the system due to practical construction tolerances. Other reasons may be found in the error tolerances of the measurement devices occasionally adding up to worst case conditions and in the accuracy of the equivalent circuit parameters. Furthermore, additional efficiency deviations are caused by the fact that the stray load losses have been neglected. However, as will be shown in Section 4.3 (Graphical Representation of Simulation Results) the simulated results correlate well with the experimental results.

Speed (rpm)	Efficiency (%)	Torque (Nm)	P_{out} (kW)	I_s (A)	p.f.	I_{Rex} (A)	I_{Lex} (A)
1202	70.81	32.5	2.90	33.26	0.104	0.6	1.1
1203	78.39	44.2	4.37	34.2	0.153	1.0	1.6
1205	84.5	63.1	6.73	36.2	0.222	1.7	2.3
1210	89.1	95.6	10.80	40.2	0.321	3.8	3.2
1215	90.96	124.3	14.38	43.2	0.399	6.0	3.5
1225	92.61	185.1	22.00	49.2	0.535	10.2	3.7
1250	92.84	342.8	41.65	68.6	0.726	20.6	3.7
1275	91.6	496.6	60.74	91.5	0.794	30.6	3.7
1300	90.0	640.1	78.45	115.2	0.815	40.3	3.7

Table 4.1 Simulated Results of R/L Controller Generator System (80 kW)

Speed (rpm)	Efficiency (%)	Torque (Nm)	P_{out} (kW)	I_s (A)	p.f.
1201	73.4	39.3	3.63	32.8	0.133
1202	85.4	72.5	7.79	34.0	0.274
1203	89.8	105.6	11.94	36.0	0.397
1204	92.0	138.6	16.08	38.7	0.497
1205	93.3	171.6	20.24	41.9	0.577
1210	95.6	333.9	40.46	62.3	0.777
1213	96.0	428.1	52.17	76.2	0.820
1220	95.9	650.1	79.6	114.1	0.850

Table 4.2 Simulated Results of Rotor Shorted Generator System (80 kW)

Speed (rpm)	P_{R1} (W)	P_{Rfe} (W)	P_{R2} (W)	P_{Rex} (W)	P_{Lex} (W)
1202	73	485	2	1	2
1203	77	485	5	3	4
1205	86	485	12	10	9
1210	103	484	26	37	16
1215	123	484	52	114	21
1225	160	484	113	335	23
1250	311	483	384	1357	24
1275	553	482	822	3009	24
1300	876	479	1405	5211	24

Table 4.3 Simulated Losses (80 kW)

4.1.1.2 Generator System of 186 kW Rating

Also for the 186 kW unit, simulation results were obtained which correspond well with the experimental ones. Especially at higher speed the results are very close to the experimental ones and are, for the most part, within ± 3%. The same reasons as mentioned in the previous Section are the cause of possible deviations.

Speed (rpm)	Efficiency (%)	Torque (Nm)	P_{out} (kW)	I_s (A)	p.f.	I_{Rex} (A)	I_{Lex} (A)
1205	76.9	144.0	13.99	101.3	0.173	3	8
1210	85.9	248.4	27.04	113.4	0.299	5	15
1215	88.4	322	36.20	126.6	0.359	8	20
1220	89.2	371	42.37	138.0	0.385	12	24
1225	89.6	408.2	46.90	147.4	0.400	15	27
1250	89.5	540.6	63.31	174.0	0.457	31	33
1275	88.9	686.6	81.47	192.8	0.531	47	34
1300	88.0	847.9	101.51	212.5	0.600	63	35
1325	86.8	1016.7	122.44	234.4	0.656	78	35
1350	85.5	1188.6	143.72	258.1	0.699	94	35
1375	84.2	1361.4	165.05	283.3	0.732	110	35
1400	82.9	1533.4	186.22	309.5	0.756	126	35

Table 4.4 Simulated Results of R/L Controlled Generator System (186 kW)

Speed (rpm)	Efficiency (%)	Torque (Nm)	P_{out} (kW)	I_s (A)	p.f.
1201	71.4	114.3	10.26	97.4	0.132
1202	84.4	212.5	22.58	101.2	0,280
1203	89.1	310.7	34.89	107.4	0.408
1204	91.5	409.1	47.19	115.6	0.512
1205	92.9	507.3	59.47	125.5	0.595
1207	94.4	703.4	83.93	148.7	0.708
1209	95.1	898.5	108.20	175.1	0.776
1211	95.5	1092.1	132.23	203.2	0.817
1213	95.6	1283.6	155.94	232.3	0.843
1216	95.7	1565.9	190.78	277.1	0.864

Figure 4.5 Simulated Results of Rotor Shorted Generator System (186 kW)

Speed (rpm)	P_{R1} (W)	P_{Rfe} (W)	P_{R2} (W)	P_{Rex} (W)	P_{Lex} (W)
1205	293	1876	18	13	36
1210	367	1868	63	53	126
1215	457	1857	119	126	233
1220	543	1646	174	237	330
1225	619	1837	226	390	411
1250	863	1815	434	1708	603
1275	1059	1809	662	3942	659
1300	1287	1805	954	7068	681
1325	1566	1802	1320	11074	691
1350	1899	1798	1762	15942	695
1375	2287	1793	2278	21651	695
1400	2729	1788	2867	28178	695

Table 4.6 Simulated Losses (186 kW)

4.1.2 Graphical Representation of Simulation Results

Figs. 4.2 to 4.6 present in a graphical way the simulation results of both the 80 kW and 186 kW generator units. When compared with the actual test results in Chapter 3.2.3 (Figs. 3.3 to 3.7), the relative validity of the steady state simulations is evident. All the graphs show good correspondence between predicted and tested ones; no severe deviations are visible.

The slight dent of the "p.f. (R/L controlled)" curve in Fig. 4.3 results from the small dc resistance of the external inductor R_{L_ex}. The smaller R_{L_ex} gets the more distinct is this dent. It is caused by the fact that both the p.f. and the output power are functions of the slip.

Consequently, instead of practical tests the derived steady state simulation model may be used for possible future research. It enables a pre-selection of specific applications and keeps the research expenses and the time effort in an acceptable frame.

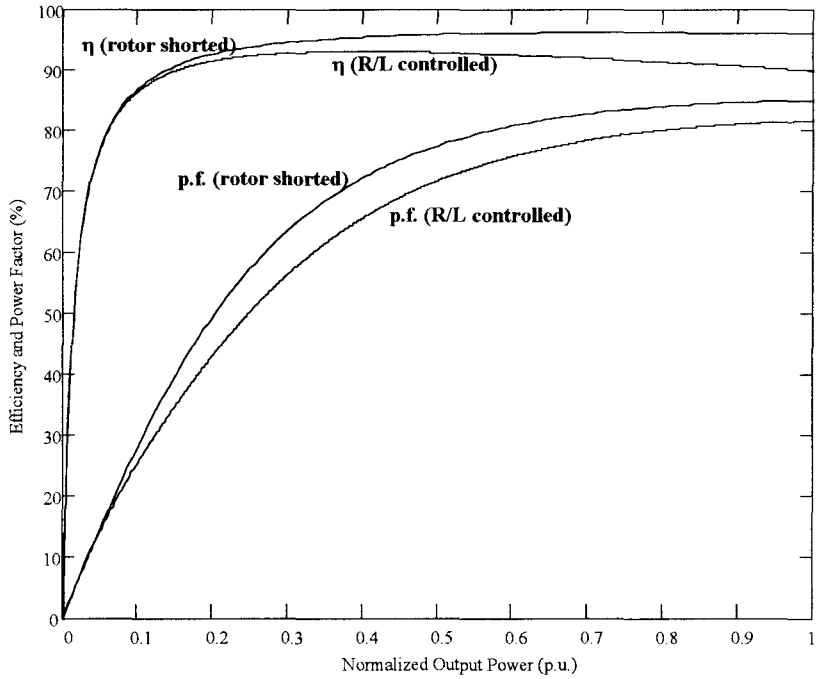

Figure 4.2 Simulated Efficiency and Power Factor (80 kW)

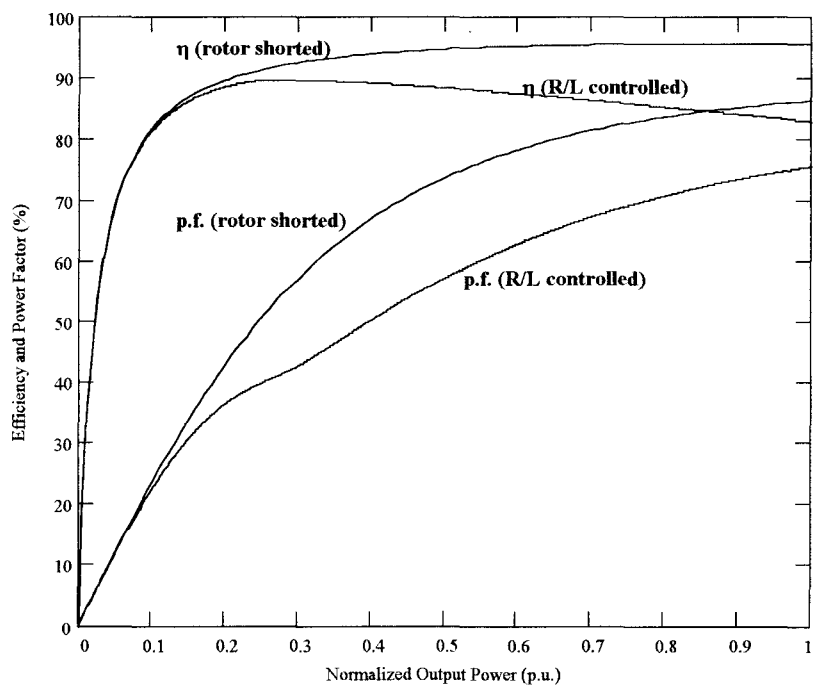

Figure 4.3 Simulated Efficiency and Power Factor (186 kW)

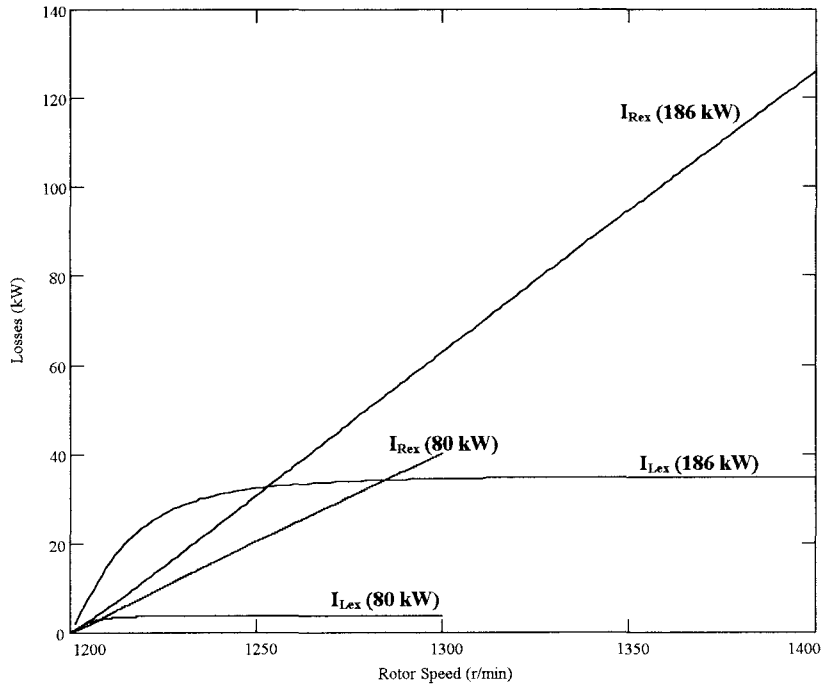

Figure 4.4 Simulated External Rotor Currents (80 and 186 kW)

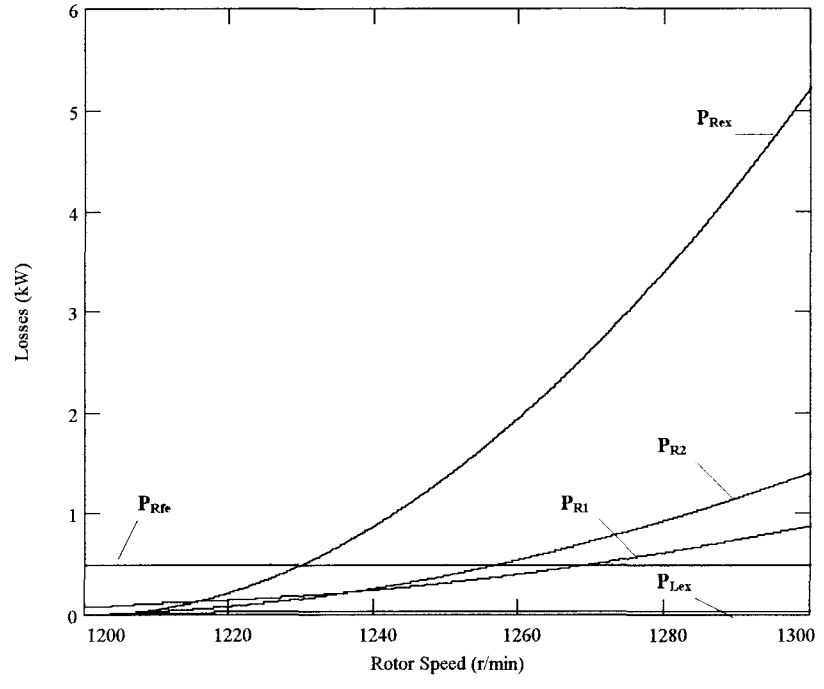

Figure 4.5 Simulated Losses (80 kW)

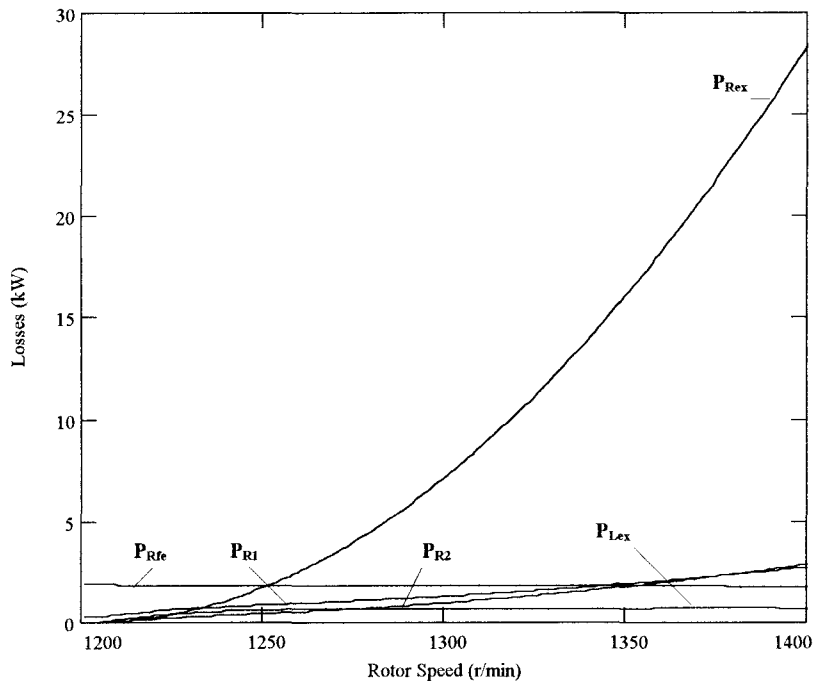

Figure 4.6 Simulated Losses (186 kW)

4.2 Dynamic Simulations

4.2.1 Mathematical Derivation of the Simulation Model

The dq induction machine model, in Park's coordinates, in a synchronous reference frame moving with the speed ω_s relative to the stator is well known [16, 17]. However, the modeling of the passive controlled variable-speed generator system has to be kept in the rotor reference frame [24] since the non-rotating time varying external inductance (L_{ex}) is linked to the rotating time varying rotor inductance. This reference frame, fixed to the rotor, assures that both the rotor leakage and the external inductance, rotate with the same speed as the rotor during simulation. Thus, the voltage equations using Clarke's transformation have to be derived as follows

$$\begin{bmatrix} V_{qs}^{r} \\ V_{ds}^{r} \end{bmatrix} = \frac{2}{3} \cdot \begin{bmatrix} 1 & -\frac{1}{2} & -\frac{1}{2} \\ 0 & \frac{\sqrt{3}}{2} & -\frac{\sqrt{3}}{2} \end{bmatrix} \times \begin{bmatrix} V_a \\ V_b \\ V_c \end{bmatrix} \tag{4.18}$$

where

$$\begin{aligned} V_a &= V_m \cdot \cos(wt - \theta_r) \\ V_b &= V_m \cdot \cos(wt - \theta_r + \frac{2\pi}{3}) \\ V_c &= V_m \cdot \cos(wt - \theta_r - \frac{2\pi}{3}) \end{aligned} \tag{4.19}$$

The factor $2\pi/3$, in the above equation, defines the 120^{o} degree phase shift between the three stator phases. The angle θ_r, presents the rotor position in electrical degrees and keeps the simulation in the rotor reference frame, which means that the dq axes rotate as rotor speed. A detailed derivation of the flux linkage and the rotor and stator currents equations (Equation 4.20 - 4.25) has been ignored since it is well known and is the topic of many papers [16, 17, or 24]; it is up to the interest of the reader to review it. Hence, the flux linkage equations in the rotor reference frame for the D-axis are

$$\frac{d\lambda_{ds}^{r}}{dt} = v_{ds}^{r} + \frac{r_s}{L_{ls}} \cdot \left(\lambda_{md}^{r} - \lambda_{ds}^{r}\right) + \omega_r \cdot \lambda_{qs}^{r} \tag{4.20}$$

$$\frac{d\lambda_{dr}^{'r}}{dt} = v_{dr}^{'r} + \frac{r_r^{'}}{L_{lr}^{'}} \cdot \left(\lambda_{md}^{r} - \lambda_{dr}^{'r}\right) \tag{4.21}$$

$$\lambda_{md}^{r} = L_M \cdot \left(\frac{\lambda_{ds}^{r}}{L_{ls}} - \frac{\lambda_{dr}^{'r}}{L_{lr}^{'}}\right) \tag{4.22}$$

where

$$L_M = \frac{1}{\frac{1}{L_m} + \frac{1}{L_{ls}} + \frac{1}{L_{lr}^{'}}} \tag{4.23}$$

In the above equations, L_{ls} and L_{lr} are, respectively, the stator leakage and rotor leakage inductances, L_m presents the stator magnetizing inductance, and r_s and r_r represent the

stator and rotor resistance. It should be noted that this equation algorithm is based on an equivalent induction machine circuit neglecting the core losses and, furthermore, saturation effects of the mutual flux linkage (λ_m) have not been considered in the simulations. The stator and rotor D-axis currents are

$$i^{r}_{ds} = \frac{\lambda^{r}_{ds} - \lambda^{r}_{md}}{L_{ls}} \tag{4.24}$$

$$i^{'r}_{dr} = \frac{\lambda^{'r}_{dr} - \lambda^{r}_{md}}{L^{'}_{lr}} \tag{4.25}$$

To include the external rotor elements into the simulation process a third state variable has to be introduced. Hence, this is the rotor current ($i^{'r}_{dr\_Lex}$) flowing through the external inductor (L_{ex}) as seen in the rotor branch excerpt, Fig.4.7, of the per-phase equivalent circuit.

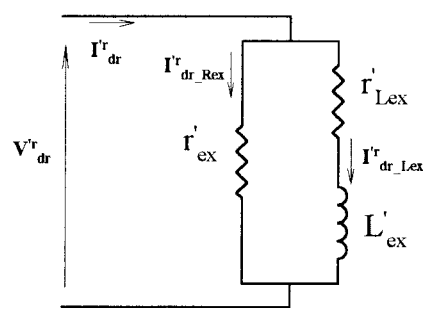

Figure 4.7 External Rotor Branch

The voltage $v^{'r}_{dr}$ of Equation (4.21) would be zero, if the slip rings of the rotor were shorted, however, in this case $v^{'r}_{dr}$ lies across the external elements and may be expressed as

$$v^{'r}_{dr} = -\left(r^{'}_{ex} \cdot i^{'r}_{dr\_Rex}\right) \tag{4.26}$$

or as

$$v'^{r}_{dr} = -\left(L'_{ex} \cdot \frac{di'^{r}_{dr\_Lex}}{dt} + r'_{Lex} \cdot i'^{r}_{dr\_Lex} \right) \tag{4.27}$$

and the rotor current (i'^{r}_{dr}) is the sum of the currents flowing through the external resistor and inductor

$$i'^{r}_{dr} = i'^{r}_{dr\_Rex} + i'^{r}_{dr\_Lex} \tag{4.28}$$

The negative sign of Equation (4.26 and 4.27) comes from the fact that the dq model rotor current (i'^{r}_{dr}) is determined to flow in the opposite direction as shown in Fig. 4.7 [16, 17, or 24]. Substituting Equation (4.26) and (4.28) into Equation (4.27) and solving for $\frac{di'^{r}_{dr\_Lex}}{dt}$ yields to the third state variable equation

$$\frac{di'^{r}_{dr\_Lex}}{dt} = \frac{r'_{ex}}{L'_{ex}} i'^{r}_{dr} - \frac{r'_{Lex} + r'_{ex}}{L'_{ex}} i'^{r}_{dr\_Lex} \tag{4.29}$$

The equations are now expressed with λ^{r}_{ds}, λ'^{r}_{dr}, and $i'^{r}_{dr\_Lex}$ as state variables for the D-axis. In the computer simulation, Equation (4.20), (4.21), and (4.29) are used to solve for λ^{r}_{ds}, λ'^{r}_{dr}, and $i'^{r}_{dr\_Lex}$ and Equation (4.22) is used to solve for λ^{r}_{md}. From Equation (4.24), (4.25), and (4.28) the currents can then be obtained.

The same algorithm can be used for the Q-axis, which leads to following equations:

Q-axis Flux Linkages

$$\frac{d\lambda^{r}_{qs}}{dt} = v^{r}_{qs} + \frac{r_s}{L_{ls}} \cdot \left(\lambda^{r}_{mq} - \lambda^{r}_{qs} \right) - \omega_r \cdot \lambda^{r}_{ds} \tag{4.30}$$

$$\frac{d\lambda'^{r}_{qr}}{dt} = v'^{r}_{qr} + \frac{r'_r}{L'_{lr}} \cdot \left(\lambda^{r}_{mq} - \lambda'^{r}_{qr} \right) \tag{4.31}$$

$$\lambda^{r}_{mq} = L_M \cdot \left(\frac{\lambda^{r}_{qs}}{L_{ls}} - \frac{\lambda^{'r}_{qr}}{L^{'}_{lr}} \right) \tag{4.32}$$

where

$$L_M = \frac{1}{\frac{1}{L_m} + \frac{1}{L_{ls}} + \frac{1}{L^{'}_{lr}}} \tag{4.33}$$

Q-axis Stator and Rotor Currents

By similar reasoning these may be expressed as

$$i^{r}_{qs} = \frac{\lambda^{r}_{qs} - \lambda^{r}_{mq}}{L_{ls}} \tag{4.34}$$

$$i^{'r}_{qr} = \frac{\lambda^{'r}_{qr} - \lambda^{r}_{mq}}{L^{'}_{lr}} \tag{4.35}$$

and

Q-axis External Voltages and Currents

$$v^{'r}_{qr} = -\left(r^{'}_{ex} \cdot i^{'r}_{qr\_Rex} \right) \tag{4.36}$$

$$v^{'r}_{qr} = -\left(L^{'}_{ex} \cdot \frac{di^{'r}_{qr\_Lex}}{dt} + r^{'}_{Lex} \cdot i^{'r}_{qr\_Lex} \right) \tag{4.37}$$

$$i^{'r}_{qdr} = i^{'r}_{qr\_Rex} + i^{'r}_{qr\_Lex} \tag{4.38}$$

$$\frac{di^{'r}_{qr\_Lex}}{dt} = \frac{r^{'}_{ex}}{L^{'}_{ex}} i^{'r}_{qr} - \frac{r^{'}_{Lex} + r^{'}_{ex}}{L^{'}_{ex}} i^{'r}_{qr\_Lex} \tag{4.39}$$

Finally, from the derived equations of the dq flux linkages and currents, the electromagnetic torque (T_{em}) of the generator can be computed, which is only equal to the mechanical torque (T_{mech}), in the steady state mode.

$$T_{em} = \frac{3}{2} \cdot \frac{p}{2} \cdot \left(\lambda^{r}_{ds} \cdot i^{r}_{qs} - \lambda^{r}_{qs} \cdot i^{r}_{ds} \right) \tag{4.40}$$

where p is the number of poles of the machine.

During dynamic operation the relation of electromagnetic and mechanical torque can be found in the equation of motion of the rotor, which depends on the inertia J, rotor speed ω_r, poles p, and the damping torque (T_{damp}) of the machine.

$$J \cdot \frac{2}{p} \cdot \frac{d\omega_r}{dt} = T_{em} - T_{mech} - T_{damp} \tag{4.41}$$

The damping torque (T_{damp}) may be expressed as

$$T_{damp} = B \cdot \omega_r \tag{4.42}$$

where B is a damping coefficient, in Nm·s, associated with the mechanical rotational system of the machine and the mechanical load. The damping factor B has been found by measuring $\frac{d\omega_r}{dt}$ at around 1200 r/min during a "running down" of the generator system (T_{em} and T_{mech} are zero). Applying $\frac{d\omega_r}{dt}$ in Equation 4.43 leads to a mean damping factor of 0.09 Nm·s for the 186 kW machine, and 0.05 Nm·s for the 80 kW machine.

$$B = \frac{J \cdot \frac{2}{p} \cdot \frac{d\omega}{dt}}{\omega_r} \tag{4.43}$$

Finally, the stator abc currents can be determined from the stator dq currents using the inverse Park transformation, Equation (4.44).

$$\begin{bmatrix} i_a \\ i_b \\ i_c \end{bmatrix} = \begin{bmatrix} \cos(-\theta_r) & \sin(-\theta_r) \\ \cos\left(-\theta_r + \frac{2\cdot\pi}{3}\right) & \sin\left(-\theta_r + \frac{2\cdot\pi}{3}\right) \\ \cos\left(-\theta_r - \frac{2\cdot\pi}{3}\right) & \sin\left(-\theta_r - \frac{2\cdot\pi}{3}\right) \end{bmatrix} \times \begin{bmatrix} i_{ds}^r \\ i_{qs}^r \end{bmatrix} \tag{4.44}$$

Thus, all the necessary equations for the computation of the dynamic performance are defined and can be programmed in the simulation process of MATLAB/SIMULINK.

4.2.2 Simulation Diagram in MATLAB/SIMULINK

Again, the dynamic simulations were carried out with MATLAB/SIMULINK as user software. It is a very simple tool to perform any kind of dynamic modeling, especially for electrical machines. The corresponding MATLAB-Files are given in Appendix C. Fig. 4.8 shows the overall simulation diagram of the generator system in which different equation sets are combined into various block diagrams. Starting from the bottom left, the integrator after the speed input signal converts the speed into the rotor angle θ_r to enable modeling in the rotor reference frame. At the output of the phase A, B, and C blocks the three phase voltages are obtained in rotor coordinates. Fig. 4.9 depicts the phase A block, which is only distinguished from the phase B, and phase C blocks by the phase shift of $\pm 120^{\circ}$, respectively.

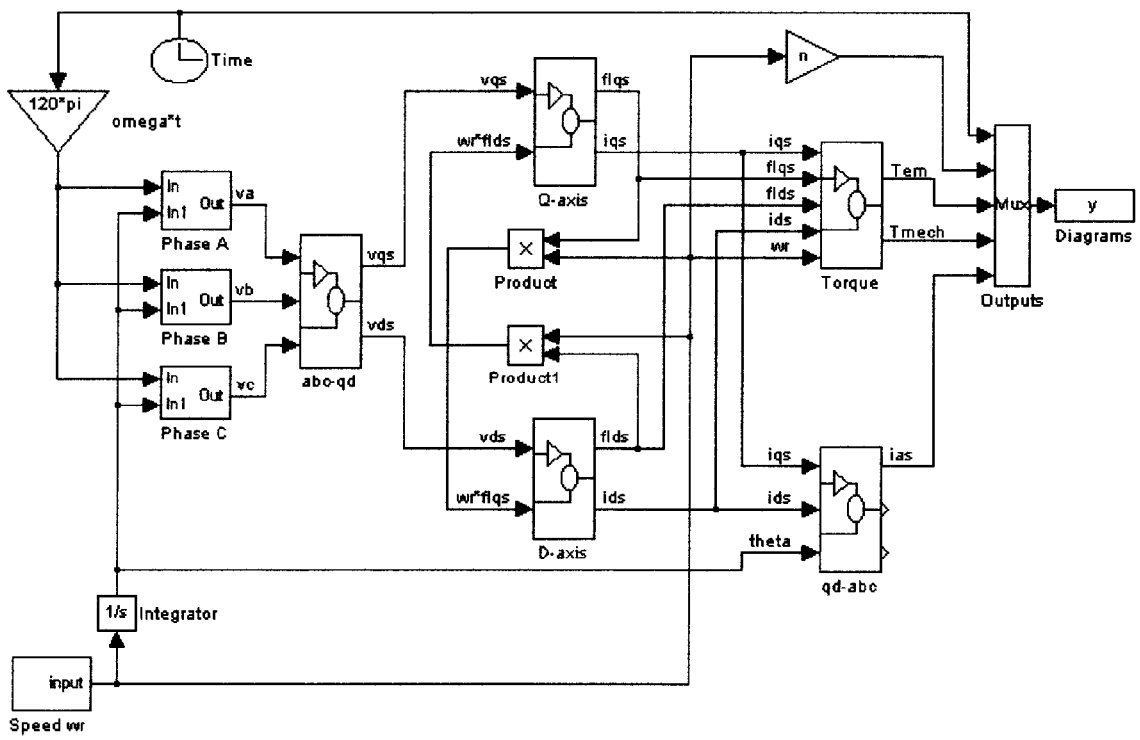

Figure 4.8 Overall Dynamic Simulation Diagram

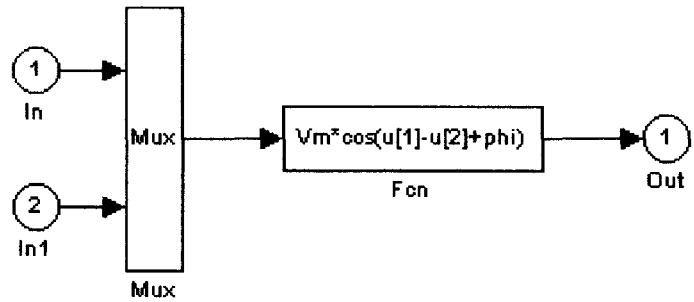

Figure 4.9 Phase A Block

Inside the abc-qd block, Fig. 4. 10, we find the transformation function from three phase abc to two phase qd to obtain v_q^r and v_d^r, using Clarke's transformation. This block actually represents Equation (4.18) which has been derived in the previous Section. Since balanced conditions and no wye-point windings connection are assumed, the zero sequence voltage v^r_o has been disregarded.

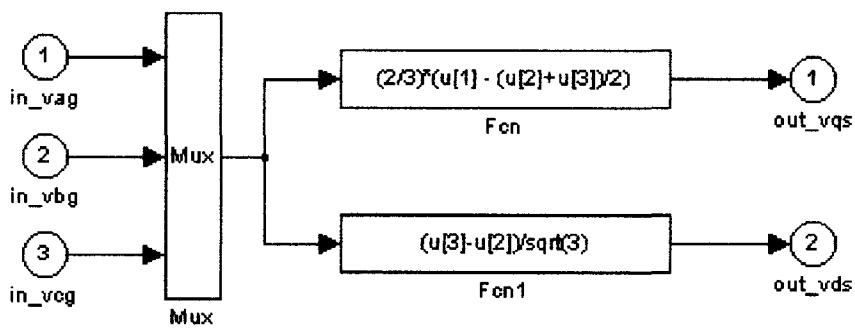

Figure 4.10 abc-qd Block

With those two voltages, the input rotor speed, and the machine parameters, the rotor and stator flux linkages and currents can be computed as shown in Fig. 4.11, the Q-axis block. Later, those values are of importance to determine the electromagnetic torque

of the generator. The Figure representing the D-axis block has been neglected, because of its similarity to the Q-axis block. Besides the replacement of the q subscript by d, the Q- and D-axis blocks differ only in their stator flux linkage equations. While the so called "speed voltage" $\omega_r \cdot \lambda'^{r}_{qs}$ for the D-axis is positive, as seen in Equation (4.20), the speed voltage $-\omega_r \cdot \lambda'^{r}_{ds}$ of the Q-axis is negative (Equation 4.30), which finds it's explanation in the 90° degree phase-shift of the d and q-axes. The D/Q-axis blocks are, substantially, the heart of the simulation and include the three state variables λ^{r}_{s}, λ'^{r}_{r}, and $i'^{r}_{r\_Lex}$, whose initial condition values are set to zero. Equations (4.30 - 4.39) implement the calculations for the outputs λ^{r}_{qs} and i^{r}_{qs} in Fig. 4.11.

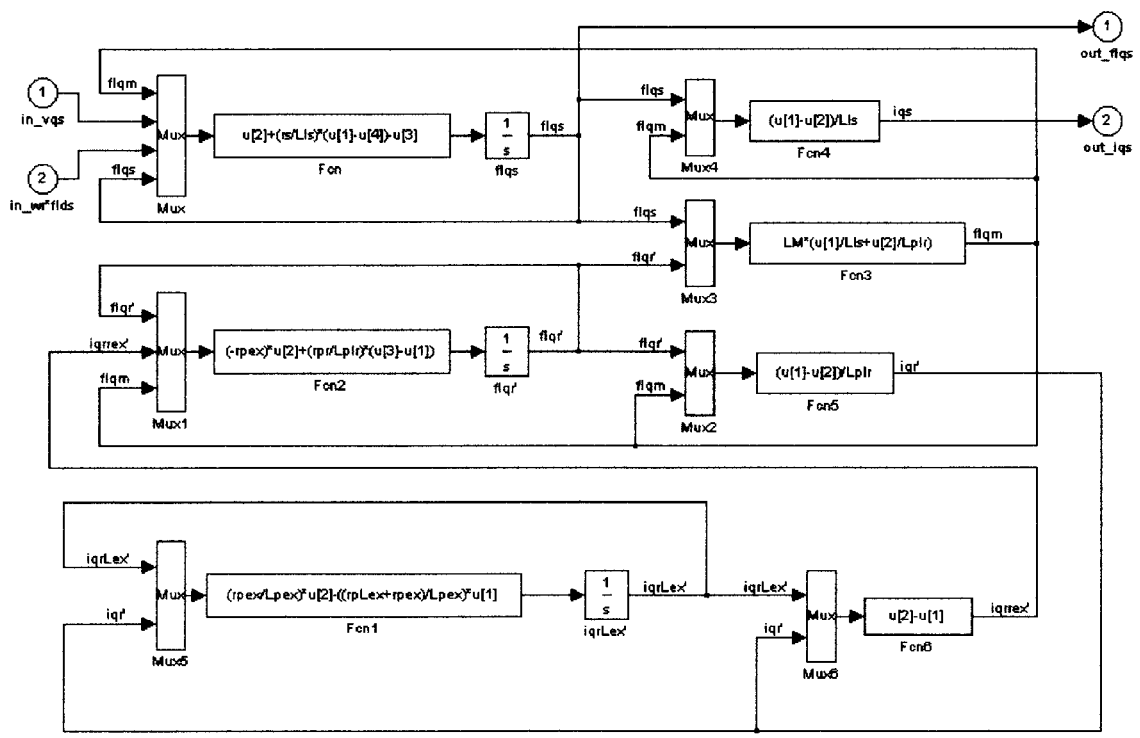

Figure 4.11 Q-axis Block

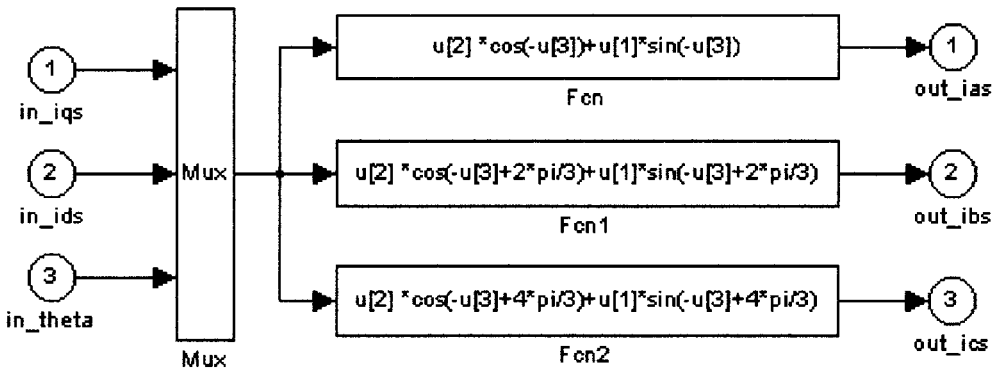

Figure 4.12 qd-abc Block

Fig. 4.12 provides the content of the qd-abc block, which enables the reverse transformation of the dq currents, rotating in the rotor reference frame, to the abc currents using the inverse Park transformation, Equation (4.43). In the simulations we concentrate only on the phase A stator current i_a, since i_b and i_c are equal in magnitude and only $\pm$ 120° phase shifted.

One more block remains, the torque block, which is illustrated in Fig. 4.13, Equations (4.41 and 4.42) are used to calculate the electromagnetic torque (T_{em}). The negative gains before the output 1 and 2 are only required to receive positive torque results, which makes the comparison to the practical tests easier. It should be noted that the actual simulated electromagnetic and mechanical torque is negative due to the derived simulation equations, which are kept in the motor mode. By applying Equation (4.41), the mechanical torque (T_{mech}) is received, where B presents the damping factor. Again it should be emphasised T_{mech} is only equal T_{em} during steady state operation.

Finally it should be explained that the "n" gain in the upper right area of Fig. 4.8 is required to convert the angular rotor speed into revolutions per minute.

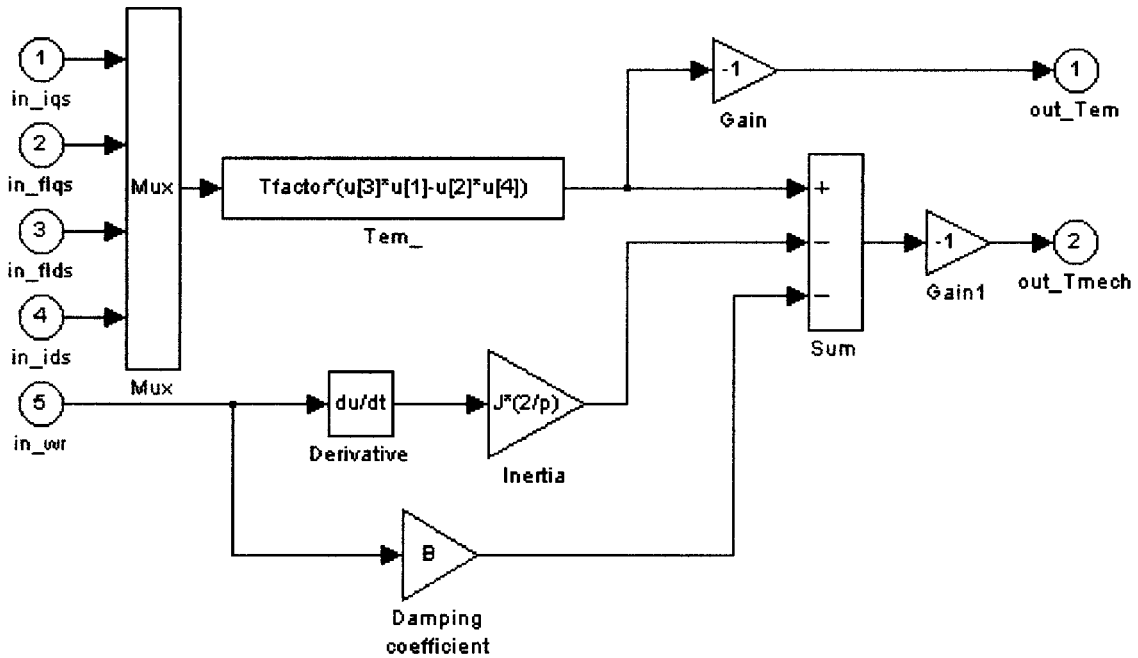

Figure 4.13 Torque Block

4.2.3 Simulation Results

The following results were obtained to represent the dynamic performance of the generators.

4.2.3.1 Generator System of 80 kW Rating

Figs. 4.14 to 4.16 illustrates the results of the MATLAB/SIMULINK simulation model. In Fig. 4.14 the results of non-synchronous connection to the power grid at a constant speed of 1225 rpm are depicted. Observing the current, a decreasing of an inrush peak of about 780 A to a steady state value of 70 A_{peak} is found, which corresponds well to the tested data (Fig. 3.8).

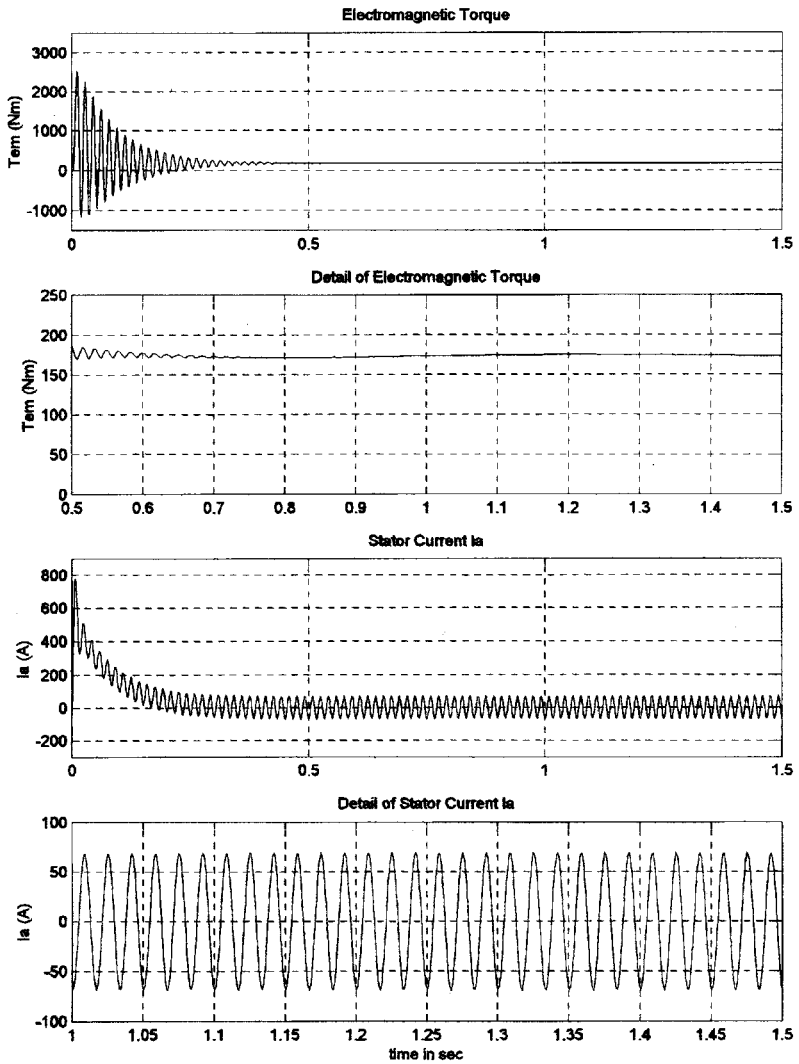

Figure 4.14 Simulated Connection to Grid at Non-Synchronous Speed (80 kW)

Also the torque stabilises to a steady state value similar to the experimental one. Only the initial torque peak of approx 2500 Nm reaches an extremely higher value compared to the tested 675 Nm. This deviation mainly comes from the inertia of the system. Since we applied a constant speed to the rotor the mechanical torque (T_{mech}) is equal to the sum of the electromagnetic torque (T_{em}) and the damping torque (T_{damp}), as also seen in Equation (4.41). Hence, the simulated mechanical torque excludes the inertia

effect and therefore is able to follow the electromagnetic torque instantaneously, resulting in a high initial torque peak.

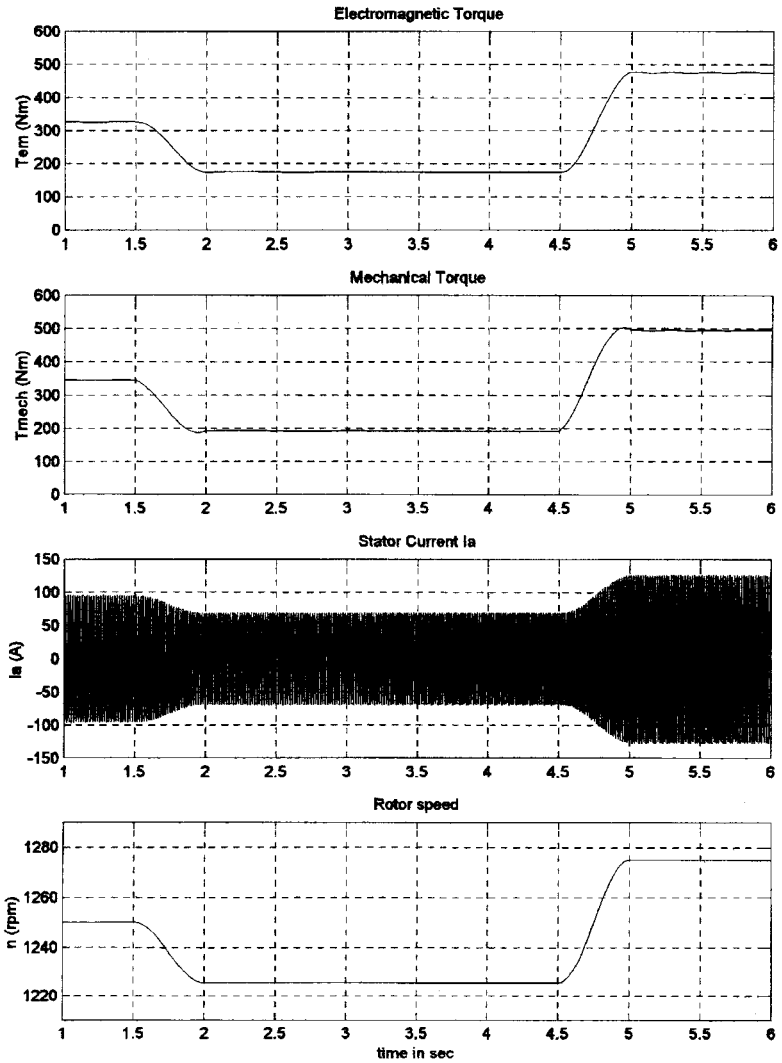

Figure 4.15 Simulated Sudden Change of Torque (80 kW)

Fig. 4.15 illustrates the simulation results to sudden changes of the applied torque to simulate wind gust situations. The simulations underwent a speed change from 1250 to 1225 to 1275 r/min, resulting in a mechanical torque change of 346 to 193 to 495 Nm,

and a stator current change of 95 to 68 to 127 A peak. Consequently, the good correlation of these simulations to the experimental results (Fig. 3.4) is evident and indicates the validity of the simulation model.

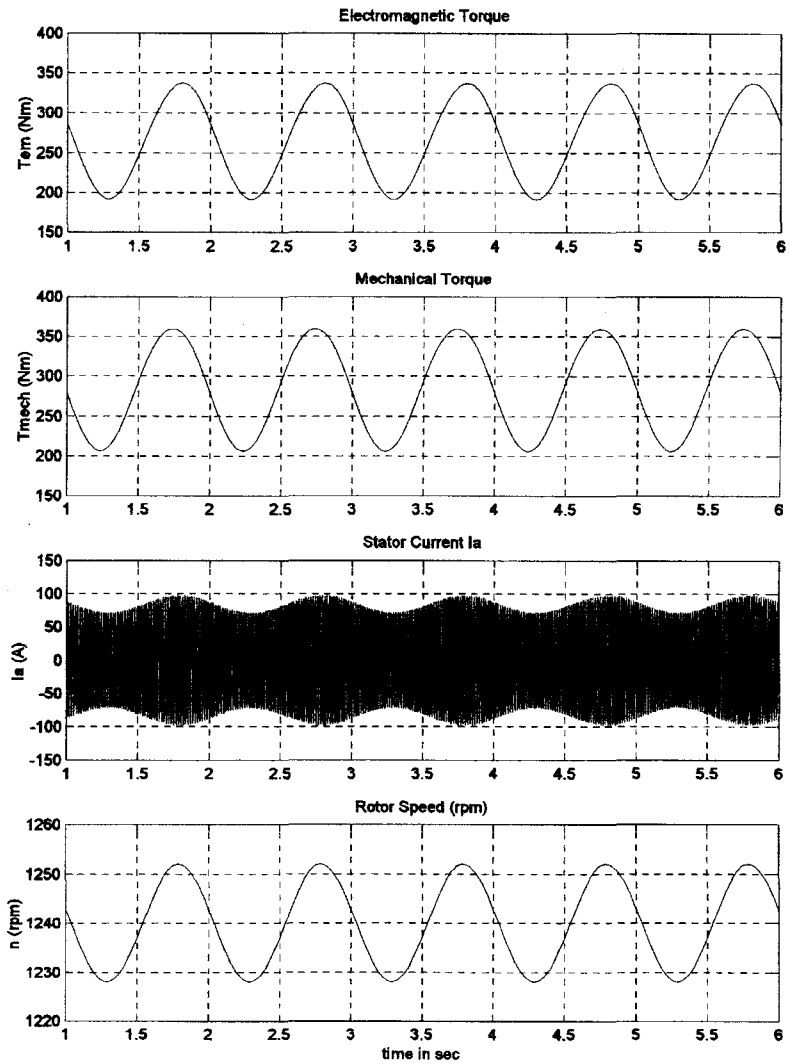

Figure 4.16 Simulated Cyclic Torque Change (80 kW)

Fig. 4.16 depicts the simulation of the generator system response to a cyclic torque variation. During simulation the system underwent a cyclic rotor speed signal with an amplitude of 12 r/min at a frequency of 1 Hz superimposed on a mean speed of 1240

r/min. The corresponding mechanical torque oscillates between 207 - 360 Nm while the current pulsates between 71 - 97 A peak. Also for this case, good simulation data has been obtained which compares well with the tested data.

4.2.3.2 Generator System of 186 kW Rating

The good correspondence between simulated and experimental results has also been received for the 186 kW generator system, which strengthens confidence in the derived simulation model. In both cases, either sudden change of torque (Fig. 4.17), or cyclic torque change (Fig. 4.18) good waveforms compared to the corresponding test data have been obtained. Only for the first simulation case, non-synchronous grid connection (Fig. 4.19), a significant deviation of the computed initial inrush torque compared to the test value has been observed, which can be attributed to the inertia effect as already explained in the previous section.

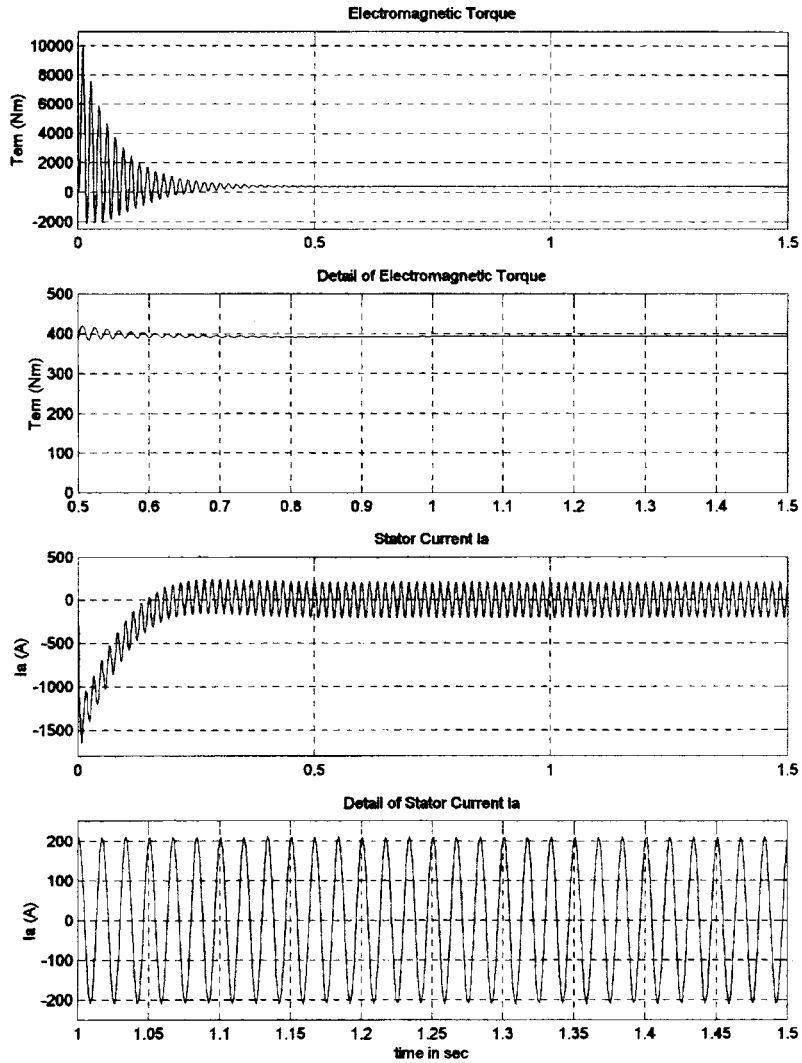

Figure 4.17 Simulated Connection to Grid at Non-Synchronous Speed (186 kW)

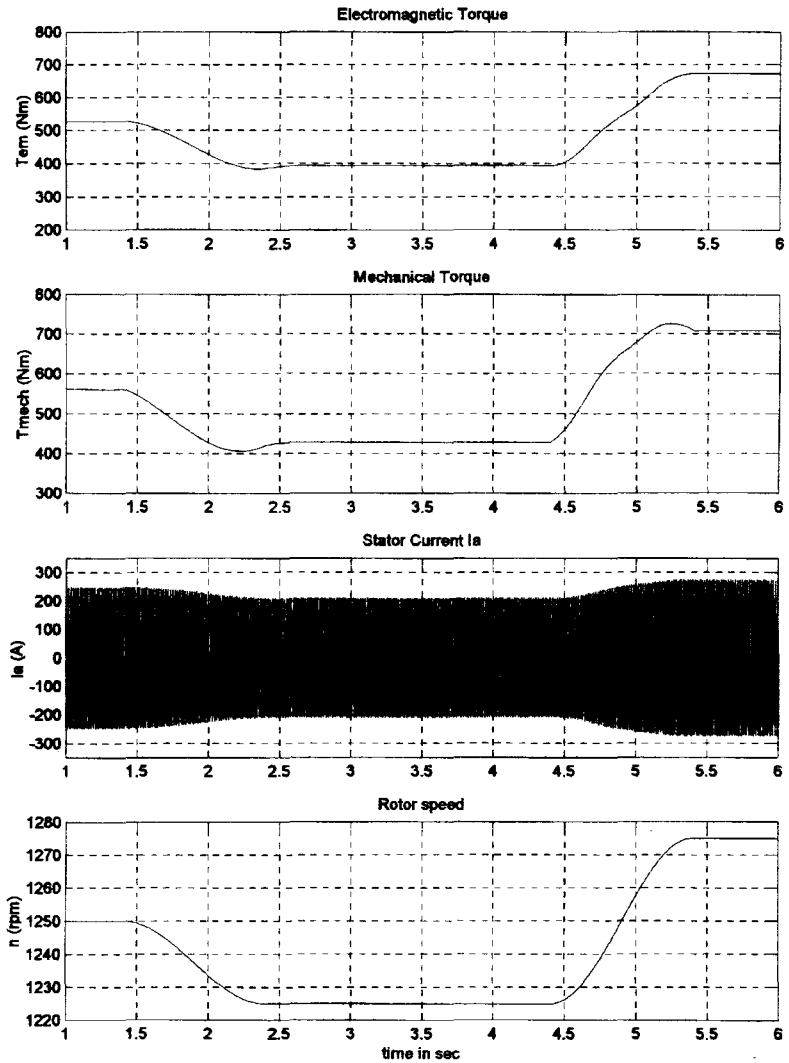

Figure 4.18 Simulated Sudden Change of Torque (186 kW)

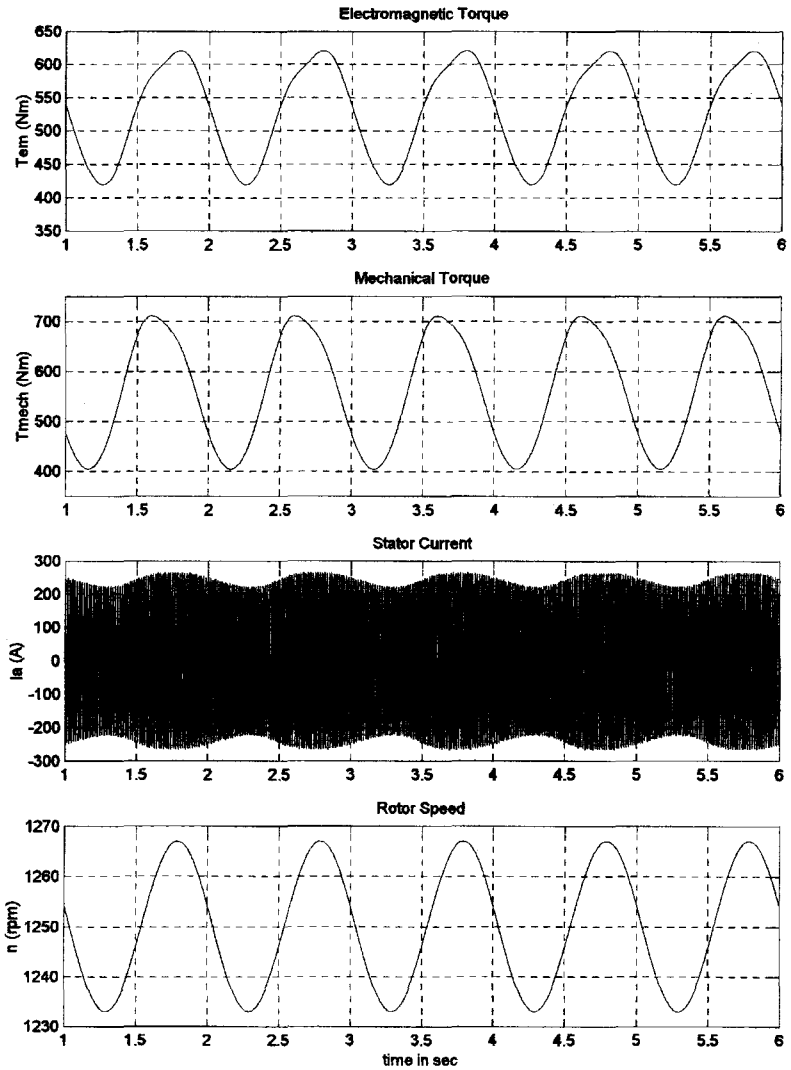

Figure 4.19 Simulated Cyclic Torque Change (186 kW)

5. CONCLUSIONS AND RECOMMENDATIONS

5.1 Conclusions

It has been shown on two generator units that an acceptable speed operation range for a variable-speed generator can be obtained by passive/external elements connected to the rotor circuit. The speed range can be arbitrarily adjusted with the passive elements. Depending on the speed operation range, efficiencies of the proposed system are comparable to those obtained by power electronic control. Especially at low speed, just above synchronous speed, efficiencies are received which are close to those of the generator alone. The proposed system should be cheaper and simpler to operate than comparable electronically controlled generator systems. Furthermore, the passively controlled system can be improved by providing rotating inductive and resistive elements, thus removing the need of slip-rings and brushes and therefore creating a unit which is virtually maintenance free; two brushless schemes are suggested in the next Section.

The dynamic tests have shown good response characteristics for a wide range of dynamic changes. Not in any of the three experiments, connecting the generator at non-synchronous speed to the power grid, sudden decreases and increases in applied torque, and cyclic torque changes, have unreasonable transients and undamped conditions been observed. This performance is valid for both generator systems (80 kW and 186 kW), operating at ranges of either 10 % or 20 % of synchronous speed. It is reasonable to assume that for system ratings other than those tested similar stability would be exhibited.

The steady state simulations performed on a typical per-phase equivalent circuit as well as the dynamic simulations performed on a novel developed machine model have implied the good modeling of the passively controlled variable-speed generator system. Thus, instead of practical tests the derived simulation model may be used for possible future research. It enables a pre-selection of specific applications and keeps the research expenses and the time effort in an acceptable frame.

5.2 Recommended Future Works

The tested and simulated results of the passively controlled variable-speed generator system were obtained using conventional wound-rotor generators with slip-rings. It is obvious that those slip rings require consistent maintenance or substantial over-engineering, which is of course, combined with additional expense. In particular, the fact that wind turbines are located frequently in remote areas and are always installed on high towers, results in relatively high maintenance expenses and which therefore is undesirable. To overcome this permanent cost, two possible ideas are proposed to receive a total brushless generator system. They are:

1) direct shaft mounting of the control elements;

2) transformer coupling to replace the slip-rings.

In the first case, the passive/external elements would be mounted directly on the rotor and therefore would be rotating with the generator shaft. In the second case, the passive/external element would be coupled over a rotating transformer to the rotor windings and placed on the stator frame. It is anticipated that both suggestions could be housed in a space only slightly larger than that required for the slip-rings, brush gear, and connection box which would be replaced.

Another recommendation for future work is the development of a mathematical model to find optimum passive/external elements. It could substitute conventional iterative methods and should be programmed in such a way as to be applicable for any passively controlled variable-speed generator system.

It is hoped to find research and development of those ideas in future theses.

BIBLIOGRAPHY

[1] A.K. Wallace, and J.A. Oliver, "Variable-Speed Generation Controlled by Passive Elements", Int. Conf. Elect. Machines, 1998, pp. 1554-1559

[2] E. Spooner and A. Williamson, "Modular Permanent-Magnet Wind-Turbine Generators", IEEE, Conference Record 31st Industrial Applications Society Annual meeting, 1996, pp. 497-502

[3] J.A. Halliday, "Wind Energy: An Option for U.K.?", IEE Proc.Vol. A, No.140, 1993, pp. 53-62

[4] P. Lampola, J. Perho, and J. Saari, "Electromagnetic and Thermal Design of Low-Speed Permanent-Magnet Generator", Proc. IEEE Powertech Conf, 1995, pp. 211-215

[5] A. Masmondi, A. Toumi, M. Kamoun, and M. Polojadoff, "Power Flow Analysis and Efficiency Optimization of Doubly-Fed Synchronous Machine", Electrical Machines and Power Systems, Vol. 21-No. 4, 1993, pp. 473-491

[6] H.K. Lauw, N.G. Klaasens, N.G. Butler, and D.B. Seeley, "Variable-Speed Generator with the Series Resonant Converter", IEEE Trans. on Energy Conversion, Vol. 3, 1988, pp. 755-764

[7] R.D. Richardson, and W.L. Erdman, "Variable Speed Wind Turbine", 1992, U.S. Patent No. 5,083,039

[8] "Rotary Induction Generator Adapted to be Driven by a Prime Mover for Generating Electric Power", 1996, U.S. Patent No. 5,525,894

[9] "Rotary Induction Machine Having Control of Secondary Winding Impedance", 1996, U.S. Patent No. 5,587,643

[10] A.K. Wallace and T.E. Rollman, "High Effiiency Testing Laboratory for Motors, Drives and Generators", IEE-PEVD, 1996, pp. 220-225

[11] A.K. Wallace, A. von Jouanne, and T. Rollman, "A Fully Regenerative, High Power Testing Facility for Motors, Drives & Generators", Oregon State University, 1997

[12] T. Lewis, D. Heberle, and A.K. Wallace, "Development of a Fully Regenerative 300 Hp Motor and Drive Test Facility", IEEE/KTH Stockholm Power Tech, 1995

BIBLIOGRAPHY (Continued)

[13] T.K. Rodrigues, "Computerrised Dynamic Control of an AC dynamometer", Thesis, Oregon State University, 1998

[14] User's Guide 1995, "Mathcad 6.0", MathSoft, Inc

[15] Simulink, "Dynamic System Simulation Software User's Guide", The Math Works

[16] P.C. Krause, O. Wasynczuk, and S.D. Sudhoff, "Analysis of Electrical Machinery" IEEE Press, New York, 1995

[17] C.M. Ong, "Dynamic Simulation of Electrical Machinery", Prentice Hall PTR, New Jersey, 1997

[18] P. Pillay and V. Levin, "Mathematical Models for Induction Machines", IEEE, 1995

[19] G.R. Slemon, "Modelling of Induction Machines for Electric Drives", IEEE, 1988

[20] G.R. Slemon, A. Stranghen, "Electric Machines", Addison Wesley, 1980

[21] M.G. Say, "The Performance and Design of Alternating Current Machines", Pitman, 1961

[22] A.E. Fitzgerald, C. Kingsley, and S. Umans, "Electric Machinery", McGraw-Hill, 1983

[23] W. Shepard and G.R. Slemon, "Rotor Impedance Control of the wound-rotor Induction Motor", Trans. AIEE, 1953, pp. 807-814

[24] D.S. Brereton, D.G. Lewis, and C.G. Young, "Representation of Induction Motor Loads During Power System Stability Studies", AIEE Trans., Vol. 76, 1957, pp.451-461

[25] P. Migliori, "Personal Communication, unpublished" National Renewable Energy Laboratory

APPENDICES

APPENDICES

APPENDIX A: Motor System Resource Facility (MSRF)

The manufacturer data of the dynamometer system and the measurement devices used during the practical tests at MSRF are listed below. Furthermore, a calibration example of the torque/speed measurement system is given.

Dynamometer System

Converter

Manufacturer:	Kenetech Windpower, Livemore, CA
Model:	MD-300
Volts:	480 V
Full load current:	350 A
Horsepower:	300 hp
Frequency range:	0 to 135 Hz
Phases:	3
Duty:	Cont
Serial No.:	001

Dynamometer

Manufacturer:	Marathon Electric Co., Wausau, WI
Model:	1K 447THDN4038 AA-W
Type:	Wound rotor induction machine
Volts:	460 V
Full load current:	332 A
Horsepower:	300 hp
r/min:	0 to 4,000 hp

Poles: 4

Duty: Cont

Serial No.: 41890480-9/16

Measurement Devices

Torque Calibration Example

Table A shows a calibrations example, which were actually adjusted for the 80 kW generator test. It includes the actual calibrated torque, the ideal torque and the error in percent. The non-linearity of the torque/speed transducer is evident. Similar calibration conditions were adjusted for the 186 kW unit.

Calibrated Torque (Nm)	Ideal Torque (Nm)	Error in %
59.8	59.78	+ 0.03
119.7	119.56	+ 0.12
179.6	179.34	+ 0.14
239.5	239.13	+ 0.15
359.2	358.69	+ 0.14
477.9	478.25	- 0.07
598.8	597.81	+ 0.17
717.4	717.38	- 0.00
955.8	956.6	- 0.08

Table A Torque Calibration Example

Torque and Speed Measurement System

Manufacturer:	Eaton Corp. - Lebow Products
Model:	1804-1K transducers, 7530-115 signal conditioner
Torque Rating:	1,000 lb-in
Nonlinearity:	± 0.05 % of full scale
Nonrepeatablity:	± 0.025 % of full scales
Hysteresis:	0.05 % of full scale
Temp. Compensated:	70 ° F to 170 ° F
Speed Range:	0-27,000 r/min
Definition:	60 pulses per rev
Error:	< 1 count per second

Power Analyser

Manufacturer:	Voltech
Model:	PM 3300 Power Analyser
Serial No.:	9463
Specified Accuracy at DC and 45 to 450 Hz:	
Voltage and Current:	0.05 % reading
	+ 0.05 % range
Power, VA, and VAR:	0.1 % reading
	+ 0.1 % range

Oscilloscope

Manufacturer:	Tektronix
Model:	TDS 460 A
Serial No.:	B020686
Frequency:	0 to 400 MHz
Accuracy:	± 1.5%

Channels:	4

AC Current Probe

Manufacturer:	Fluke
Model:	80i-1000s
Serial No.:	67963900
Frequency:	5 to 100 kHz
Inputs:	0.1 to 1000 A
Isolation from Earth:	600 V

APPENDIX B: Nameplate Details of 80 kW and 186 kW Machines

In this section the detailed nameplate data and the Y-connected per-phase equivalent circuit parameter of the 80 kW and 186 kW generator are listed.

80 kW Generator

Manufacturer:	Reliance DE Mexico, S.A.
Design:	Slip-ring Wound Rotor Induction Motor
Serial No.:	B2096201211
Frame/Enclosure:	445T/WPI
Insulation:	H
Service Factor:	1.15
Time Rating:	Continuous
Temp. Rise:	80° C
Max. Amb. Temp:	50° C
kW:	80
r/min:	1212
Volts:	480
Amps:	114
Hertz/Phases	60/3
Rotor-stator ratio:	2.5
R_1:	0.0022 Ω
X_1:	0.12 Ω
R_{fe}:	466 Ω
X_m:	8.47 Ω
R'_2:	0.045 Ω
X'_2:	0.603 Ω

186 kW Generator

Manufacturer:	Marathon Electric, Warsau, WC
Design:	Slip-ring Wound Rotor Induction Motor
Serial No.:	MU170960-115
Model:	5A 508UHDS7087AN W
Frame:	508USZ
Type:	KDS
Class of Insulation:	H
Service Factor:	1.0
Max. Amb. Temp.:	40° C
kW:	186
r/min:	1180
Volts:	460
Amps:	290
Hertz/phases:	60/3
Rotor-stator ratio:	2.01
R_1:	0.0095 Ω
X_1:	0.0893 Ω
R_{fe}:	105.429 Ω
X_m:	2.667 Ω
R'_2:	0.0133 Ω
X'_2:	0.0848 Ω

APPENDIX C: Dynamic Simulation M-files

All the M-files for the dynamic simulations of both generators performed in MATLAB/SIMULINK are listed below.

Generator System of 80 kW

ap80kW.m file

```
% M-file of machine parameters of machine used in 80 kW simulations
Vrated = 480;                       % rated line to line voltage in V
phi = 1.12*pi;                      % starting phase angle of stator voltage
p = 6;                              % number of poles
frated = 60;                        % rated frequency in Hz
a = 2.5;                            % rotor/stator turn ration
Vm = Vrated*sqrt(2/3);              % magnitude of phase voltage
Tfactor = (3*p)/4;                  % factor for torque expression
rs = 0.022;                         % stator wdg resistance in ohms
Lls = 0.000318;                     % stator leakage reactance in ohms
Lm = 0.02247;                       % stator magnetizing reactance
rpr = 0.045;                        % referred rotor wdg resistance in ohms
Lplr = 0.00159;                     % rotor leakage reactance
rpex = 1.1/(a*a);                   % external (passive) resistor
rpLex = 0.57/(a*a);                 % external (passive) resistance of the coil
Lpex = 0.368/(a*a);                 % external (passive) inductance
LM = 1/(1/Lm + 1/Lls + 1/Lplr);
J = 3.5;                            % rotor inertia in kg*m^2
B = 0.05;                           % rotor damping coefficient
```

ag80.m file

```
% M-file for 80 kW induction generator simulations when connecting to the power
```

```
% grid at a speed of 1225 rpm. It sets up the motor parameters, initial conditions, and
% speed input in the MATLAB workspace for simulation, and plots the results of the
% simulation.
%
% Load three-phase induction motor parameters
ap80kW                          % load 80 kW motor parameters from ap80kW.m
% initialize to start from standstill with machine unexcited
flqs = 0;                       % stator q-axis total flux linkage
flqr = 0;                       % rotor q-axis total flux linkage
flds = 0;                       % stator d-axis total flux linkage
fldr = 0;                       % rotor d-axis total flux linkage
iqrLex = 0;                     % external q-axis inductance current
idrLex = 0;                     % external d-axis inductance current
tstop = 1.5;                    % use 1.5 sec simulation time for Fig. in text
% Transfer to keyboard for simulation
disp('Set up for running as_g80.m');
as_g80;
sim('as_g80');
close all;
% Plot commands
figure(20);
subplot(4,1,1)
plot(y(:,1),y(:,3),'-')
axis([0 1.5 -1500 3500]);
ylabel('Tem (Nm)')
title('Electromagnetic Torque')
grid on;
subplot(4,1,2)
plot(y(:,1),y(:,3),'-')
axis([0.5 1.5 0 250]);
ylabel('Tem (Nm)')
```

```
title('Zoomed Electromagnetic Torque')
grid on;
subplot(4,1,3)
plot(y(:,1),y(:,5),'-')
axis([0 1.5 -300 900]);
ylabel('Ia (A)')
title('Stator Current Ia')
grid on;
subplot(4,1,4)
plot(y(:,1),y(:,5),'-')
axis([1 1.5 -100 100]);
ylabel('Ia (A)')
xlabel('time in sec')
title('Zoomed Stator Current Ia')
grid on;
```

avs80.m file

```
% M-file for 80 kW induction machine simulations when varying the speed from 1250 -
% 1225 - 1275 rpm. It sets up the motor parameters, initial conditions, and mechanical
% loading in the MATLAB workspace for simulation, and plots the results of the
% simulation.
%
% Load three-phase induction motor parameters
ap80kW                          % load 80 kW motor parameters from ap80kW.m
% initialize to start from standstill with machine unexcited
flqs = 0;                       % stator q-axis total flux linkage
flqr = 0;                       % rotor q-axis total flux linkage
flds = 0;                       % stator d-axis total flux linkage
fldr = 0;                       % rotor d-axis total flux linkage
iqrLex = 0;                     % external q-axis inductance current
idrLex = 0;                     % external d-axis inductance current
```

```
tstop = 6;                          % use 6 sec simulation time for Fig. in text
n = 60/(2*pi*3);                    % factor to see speed in rpm
% Transfer to keyboard for simulation
disp('Set up for running as_vs80.m');
as_vs80;
sim('as_vs80');
close all;
% Plot commands
figure(20);
subplot(4,1,4)
plot(y(:,1),y(:,2),'-')
axis([1 6 1210 1290]);
ylabel('n (rpm)')
title('Rotor speed')
xlabel('time in sec')
grid on;
subplot(4,1,1)
plot(y(:,1),y(:,3),'-')
axis([1 6 0 600]);
ylabel('Tem (Nm)')
title('Electromagnetic Torque')
grid on;
subplot(4,1,2)
plot(y(:,1),y(:,4),'-')
axis([1 6 0 600]);
ylabel('Tmech (Nm)')
title('Mechanical Torque')
grid on;
subplot(4,1,3)
plot(y(:,1),y(:,5),'-')
axis([1 6 -150 150]);
```

```
ylabel('Ia (A)')
title('Stator Current Ia')
grid on;
```

asin80.m file

```
% M-file for 80 kW induction machine simulations when applying a sinusoidal speed
% input. It sets up the motor parameters, initial conditions, and speed input in the
% MATLAB workspace for simulation, and plots the results of the simulation.
%
% Load three-phase induction motor parameters
ap80kW                          % load 80 kW motor parameters from ap80kW.m
n = 60/(2*pi*3);                % factor to see speed in rpm
% initialize to start from standstill with machine unexcited
flqs = 0;                       % stator q-axis total flux linkage
flqr = 0;                       % rotor q-axis total flux linkage
flds = 0;                       % stator d-axis total flux linkage
fldr = 0;                       % rotor d-axis total flux linkage
iqrLex = 0;                     % external q-axis inductance current
idrLex = 0;                     % external d-axis inductance current
tstop = 6;                      % use 6 sec simulation time for Fig. in text
% Transfer to keyboard for simulation
disp('Set up for running as_sin80.m');
as_sin80;
sim('as_sin80');
close all;
figure(20);
% Plot commands
subplot(4,1,4)
plot(y(:,1),y(:,2),'-')
axis([1 6 1220 1260]);
ylabel('n (rpm)')
```

```
title('Rotor Speed (rpm)')
xlabel('time in sec')
grid on;
subplot(4,1,1)
plot(y(:,1),y(:,3),'-')
axis([1 6 150 400]);
ylabel('Tem (Nm)')
title('Electromagnetic Torque')
grid on;
subplot(4,1,2)
plot(y(:,1),y(:,4),'-')
axis([1 6 150 400]);
ylabel('Tmech (Nm)')
title('Mechanical Torque')
grid on;
subplot(4,1,3)
plot(y(:,1),y(:,5),'-')
axis([1 6 -150 150]);
ylabel('Ia (A)')
title('Stator Current Ia')
grid on;
```

Generator System of 186 kW

ap250hp.m file

```
% M-file of machine parameters used in 186 kW (250hp) simulations
Vrated = 460;                % rated line to line voltage in V
phi = 0;                     % starting phase angle of stator voltage
p = 6;                       % number of poles
frated = 60;                 % rated frequency in Hz
a = 2.01;                    % rotor/stator turn ration
```

```
Vm = Vrated*sqrt(2/3);          % magnitude of phase voltage
Tfactor = (3*p)/4;              % factor for torque expression
rs = 0.0095;                    % stator wdg resistance in ohms
Lls = 0.000237;                 % stator leakage reactance in ohms
Lm = 0.007074;                  % stator magnetizing reactance
rpr = 0.01333;                  % referred rotor wdg resistance in ohms
Lplr = 0.000225;                % rotor leakage reactance
rpex = 0.595/(a*a);             % external (passive) resistor
rpLex = 0.19/(a*a);             % external (passive) resistance of the coil
Lpex = 0.034/(a*a);             % external (passive) inductance
LM = 1/(1/Lm + 1/Lls + 1/Lplr);
J = 9;                          % rotor inertia in kg*m^2
B = 0.09;                       % rotor damping coefficient in Nm*s
```

ag250.m file

```
% M-file for 250hp induction generator simulations when connecting to the power
% grid at a speed of 1225 rpm. It sets up the motor parameters, initial conditions, and
% speed input in the MATLAB workspace for simulation, and plots the results of the
% simulation.
%
% Load three-phase induction motor parameters
ap250hp                         % load 250 hp motor parameters from ap250hp.m
% initialize to start from standstill with machine unexcited
flqs = 0;                       % stator q-axis total flux linkage
flqr = 0;                       % rotor q-axis total flux linkage
flds = 0;                       % stator d-axis total flux linkage
fldr = 0;                       % rotor d-axis total flux linkage
iqrLex = 0;                     % external q-axis inductance current
idrLex = 0;                     % external d-axis inductance current
tstop = 1.5;                    % use 1.5 sec simulation time for Fig. in text
% Transfer to keyboard for simulation
```

```
disp('Set up for running as_g250.m');
as_g250;
sim('as_g250');
close all;
% Plot commands
figure(20);
subplot(4,1,1)
plot(y(:,1),y(:,3),'-')
axis([0 1.5 -2500 11000]);
ylabel('Tem (Nm)')
title('Electromagnetic Torque')
grid on;
subplot(4,1,2)
plot(y(:,1),y(:,3),'-')
axis([0.5 1.5 0 500]);
ylabel('Tem (Nm)')
title('Zoomed Electromagnetic Torque')
grid on;
subplot(4,1,3)
plot(y(:,1),y(:,5),'-')
axis([0 1.5 -1600 500]);
ylabel('Ia (A)')
title('Stator Current Ia')
grid on;
subplot(4,1,4)
plot(y(:,1),y(:,5),'-')
axis([1 1.5 -250 250]);
ylabel('Ia (A)')
xlabel('time in sec')
title('Zoomed Stator Current Ia')
grid on;
```

avs250.m file

```
% M-file for 250hp induction machine simulations when varying the speed from 1250 -
% 1225 - 1275 rpm. It sets up the motor parameters, initial conditions, and mechanical
% loading in the MATLAB workspace for simulation, and plots the results of the
% simulation.
%
% Load three-phase induction motor parameters
ap250hp                          % load 250 hp motor parameters from p250hp.m
% initialize to start from standstill with machine unexcited
flqs = 0;                        % stator q-axis total flux linkage
flqr = 0;                        % rotor q-axis total flux linkage
flds = 0;                        % stator d-axis total flux linkage
fldr = 0;                        % rotor d-axis total flux linkage
iqrLex = 0;                      % external q-axis inductance current
idrLex = 0;                      % external d-axis inductance current
tstop = 6;                       % use 6 sec simulation time for Fig. in text
n = 60/(2*pi*3);                 % factor to see speed in rpm
% Transfer to keyboard for simulation
disp('Set up for running as_vs250.m');
as_vs250;
sim('as_vs250');
close all;
% Plot commands
figure(20);
subplot(4,1,4)
plot(y(:,1),y(:,2),'-')
axis([1 6 1220 1280]);
ylabel('n (rpm)')
title('Rotor speed')
xlabel('time in sec')
grid on;
```

```
subplot(4,1,1)
plot(y(:,1),y(:,3),'-')
axis([1 6 200 800]);
ylabel('Tem (Nm)')
title('Electromagnetic Torque')
grid on;
subplot(4,1,2)
plot(y(:,1),y(:,4),'-')
axis([1 6 300 800]);
ylabel('Tmech (Nm)')
title('Mechanical Torque')
grid on;
subplot(4,1,3)
plot(y(:,1),y(:,5),'-')
axis([1 6 -350 350]);
ylabel('Ia (A)')
title('Stator Current Ia')
grid on;
```

asin250.m file

```
% M-file for 250hp induction machine simulations when applying a sinusoidal speed
% input. It sets up the motor parameters, initial conditions, and speed input in the
% MATLAB workspace for simulation, and plots the results of the simulation.
%
% Load three-phase induction motor parameters
ap250hp                    % load 250 hp motor parameters from p250hp.m
% initialize to start from standstill with machine unexcited
flqs = 0;                  % stator q-axis total flux linkage
flqr = 0;                  % rotor q-axis total flux linkage
flds = 0;                  % stator d-axis total flux linkage
fldr = 0;                  % rotor d-axis total flux linkage
```

```
iqrLex = 0;                          % external q-axis inductance current
idrLex = 0;                          % external d-axis inductance current
tstop = 6;                           % use 2 sec simulation time for Fig. in text
n = 60/(2*pi*3);                     % factor to see speed in rpm
% Transfer to keyboard for simulation
disp('Set up for running as_vs250.m');
as_vs250;
sim('as_vs250');
close all;
% Plot commands
figure(20);
subplot(4,1,4)
plot(y(:,1),y(:,2),'-')
axis([1 6 1220 1280]);
ylabel('n (rpm)')
title('Rotor speed')
xlabel('time in sec')
grid on;
subplot(4,1,1)
plot(y(:,1),y(:,3),'-')
axis([1 6 200 800]);
ylabel('Tem (Nm)')
title('Electromagnetic Torque')
grid on;
subplot(4,1,2)
plot(y(:,1),y(:,4),'-')
axis([1 6 300 800]);
ylabel('Tmech (Nm)')
title('Mechanical Torque')
grid on;
subplot(4,1,3)
```

```
plot(y(:,1),y(:,5),'-')
axis([1 6 -350 350]);
ylabel('Ia (A)')
title('Stator Current Ia')
grid on;
```